Notable Events

The October 2012 magnitude (Mw) 7.8 earthquake offshore Haida Gwaii, Canada

Alison L. Bird et al.

Geological Survey of Canada, Natural Resources Canada

Sidney, BC, Canada

Excerpt from the
Summary of the Bulletin of the International Seismological Centre:

Bird, A. L. et al., The October 2012 magnitude (Mw) 7.8 earthquake offshore Haida Gwaii, Canada, *Summ. Bull. Internatl. Seismol. Cent.*, July - December 2012, *49*(7–12), pp. 41–72, Thatcham, United Kingdom, 2016, doi:10.5281/zenodo.999242.

6.2 The October 2012 magnitude (M_W) 7.8 earthquake offshore Haida Gwaii, Canada

Alison L. Bird[1], John F. Cassidy[1&2], Honn Kao[1&2], Lucinda J. Leonard[1&2], Trevor I. Allen[1], Lisa Nykolaishen[1], Herb Dragert[1], Tiegan E. Hobbs[3], Amir M. Farahbod[4], Jan M. Bednarski[1], Thomas S. James[1], Maurice Lamontagne[5], Shao-Ju Shan[1], Roy D. Hyndman[1], Isaac V. Fine[6], Josef Y. Cherniawsky[6], Camille D. Brillon[1], Kelin Wang[1&2] and Garry C. Rogers[1&2]

Alison L. Bird
Geological Survey of Canada
Natural Resources Canada
Sidney, British Columbia
Canada

1. Geological Survey of Canada, Natural Resources Canada, Sidney, British Columbia, Canada.
2. School of Earth and Ocean Sciences, University of Victoria, Victoria, British Columbia, Canada.
3. School of Earth and Atmospheric Sciences, Georgia Institute of Technology, Atlanta, Georgia, Unites States of America.
4. Geological Survey of Canada, Natural Resources Canada, Vancouver, British Columbia, Canada.
5. Geological Survey of Canada, Natural Resources Canada, Ottawa, Ontario, Canada.
6. Canadian Hydrographic Service, Department of Fisheries and Oceans, Sidney, British Columbia, Canada.

6.2.1 Introduction

The Haida Gwaii archipelago (formerly known as the Queen Charlotte Islands) is located off the coast of central British Columbia (BC), Canada (Figure 6.7). While approximately 150 islands make up Haida Gwaii, there are two main islands: the northern Graham Island and southern Moresby Island; the two are separated by the narrow Skidegate Channel. Approximately 5,000 people live on Haida Gwaii, mostly in six small communities, five of them on Graham Island.

On the evening of 27th October 2012 (8:04pm local time), a magnitude (M_W) 7.8 earthquake occurred along a previously only hypothesised thrust fault off the west coast of Moresby Island. This was the second largest earthquake in Canada's written history. It was felt throughout much of British Columbia and as far away as the Yukon, Alberta and Montana, roughly 1600 km from the epicentre. In some locations (notably on Haida Gwaii) the perceivable shaking lasted 1.5 - 2 minutes, with very strong shaking for about 30 seconds. Strong ground motions recorded in the region reached a maximum horizontal acceleration of $0.2g$. Fortunately, this earthquake resulted in very limited damage partly because of the relatively large distance (more than 60 km) between population centres and the fault rupture, and partly because of seismic resistance of the generally low, wood-frame construction found on the islands. We examine the earthquake rupture characteristics and crustal displacements, along with various physical effects from the shaking (including ground motions, tsunami, landslides, building damage and the loss of hot springs), catalogued by field crews and reported by the inhabitants of Haida

Gwaii and the surrounding regions. These will serve as a guide toward understanding the potential impact from future large earthquakes on the various Haida Gwaii communities.

6.2.2 Historical Seismicity and Tectonics

The Queen Charlotte Fault (QCF), a near-vertical fault running along the west coast of Haida Gwaii and north into south-eastern Alaska, is a transpressional boundary between the Pacific and North American Plates (Bird 1997, Bird *et al.*, 1997; Figure 6.8). Little was known in detail about the distribution of earthquakes in this region before the establishment of a local seismograph network between 1982 and 1987. Some sizeable earthquakes had been recorded by the regional seismic network in previous decades, however, including a magnitude (M_W) 7 in 1929 (Milne, 1956), an M_S 8.1 event off north-western Graham Island in 1949 (the largest instrumentally recorded earthquake in Canadian history; Bostwick, 1984) and an M_W 7.4 in 1970 (Lamontagne *et al.*, 2008). The rupture zones of these events, as defined by their aftershock distribution, suggested a seismic gap (Rogers, 1986) remained along the southernmost portion of the QCF.

The network installed in the 1980's revealed not only intense seismicity along the plate boundary region but also a more extensive pattern of activity than that associated simply with the QCF, with substantial activity shown to occur up to 150 km east of the fault, in particular under Graham Island and Hecate Strait (Bird 1997, Bird *et al.*, 1997; Ristau *et al.*, 2007).

Pacific - North America relative plate motion is roughly 50 mm/year (DeMets *et al.*, 1990 and 2010; Hyndman, 2015) with a discrepancy between plate motion and fault strike of 15° to 20° – varying along-fault and greatest along the southern section of the QCF. This leads to a small, but significant component of oblique convergence at approximately 15 mm/year that is believed to have initiated at ~6 Ma, resulting in under-thrusting at the margin (Bird 1997, Bird *et al.*, 1997; Barrie *et al.*, 2013; Hyndman, 2015). The total under-thrusting has been too small to instigate Benioff-Wadati seismicity or arc volcanism but is indicated by: (1) a trench: the Queen Charlotte Trough, into which the converging oceanic plate bows downward, and an adjacent offshore flexural bulge, the Oshawa Rise; (2) the Queen Charlotte Terrace (QCT), interpreted to be an accretionary sedimentary prism; (3) seismic receiver function delineation of the under-thrusting Pacific Plate; (4) heat flow decreasing landward as predicted for under-thrusting; (5) low gravity offshore and high gravity onshore, consistent with subduction; and (6) late Tertiary uplift and erosion of the western coasts of the islands (Hyndman, 2015). Oblique convergence is partitioned into nearly margin-normal under-thrusting relative to the Terrace, which itself is moving along the margin, and margin-parallel transform motion on the Queen Charlotte Fault just off the coast, which produced the aforementioned M 8.1 earthquake in 1949.

Focal mechanisms for the region have been dominantly strike-slip, but with a considerable component of thrust, especially for earthquakes along the section of fault adjacent to Moresby Island in the south (Bird 1997, Bird *et al.*, 1997; Ristau *et al.*, 2007). This is consistent with the oblique convergence across the dominantly strike-slip QCF in the area where the fault changes strike into a somewhat more E-W orientation along this southern section of the QCF, giving the fault a dog-leg appearance.

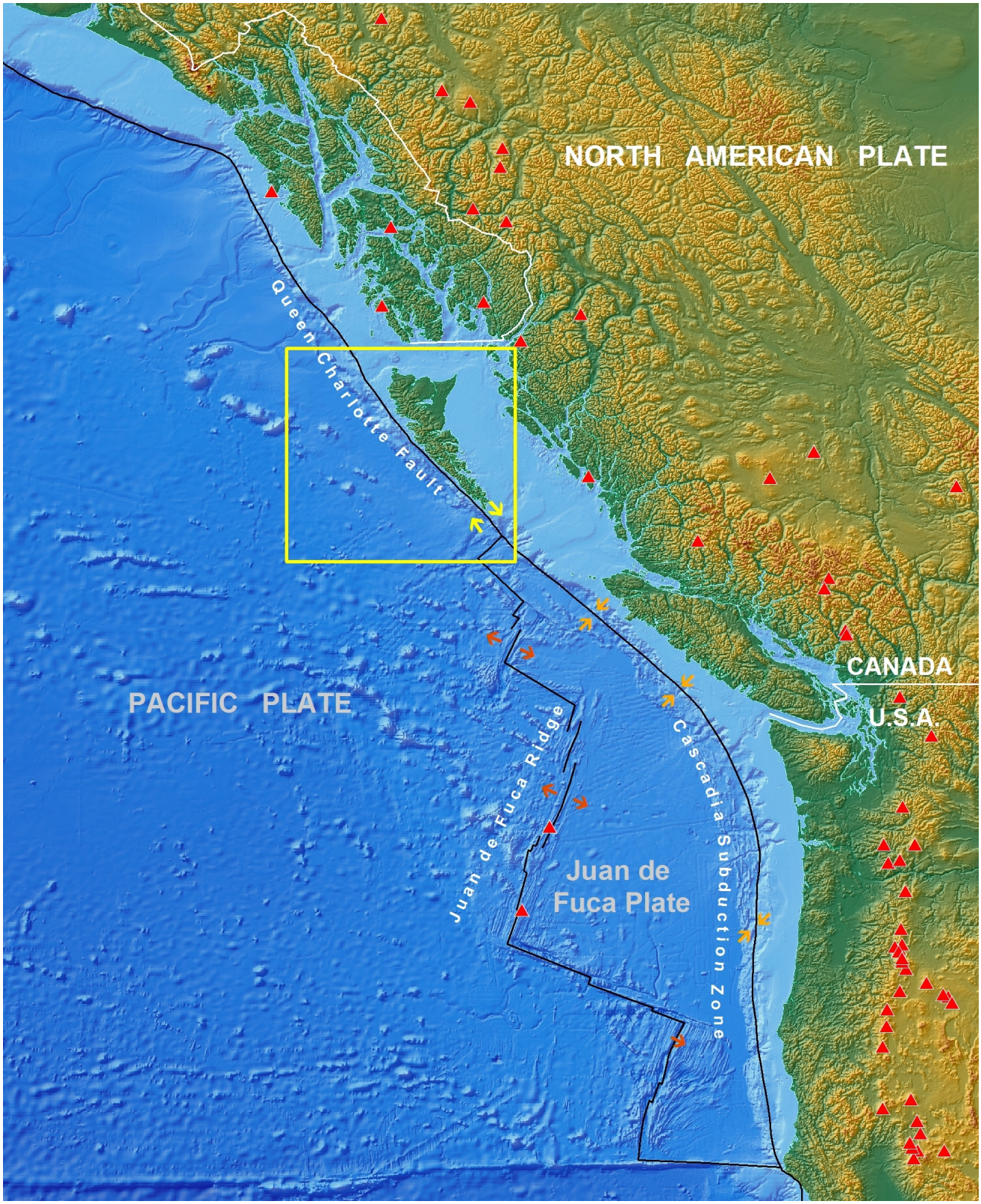

Figure 6.7: *Regional tectonic setting off the west coast of British Columbia in western Canada, with the area of study indicated by the yellow box. Arrows show relative plate motion across plate boundaries, and red triangles indicate volcanic features.*

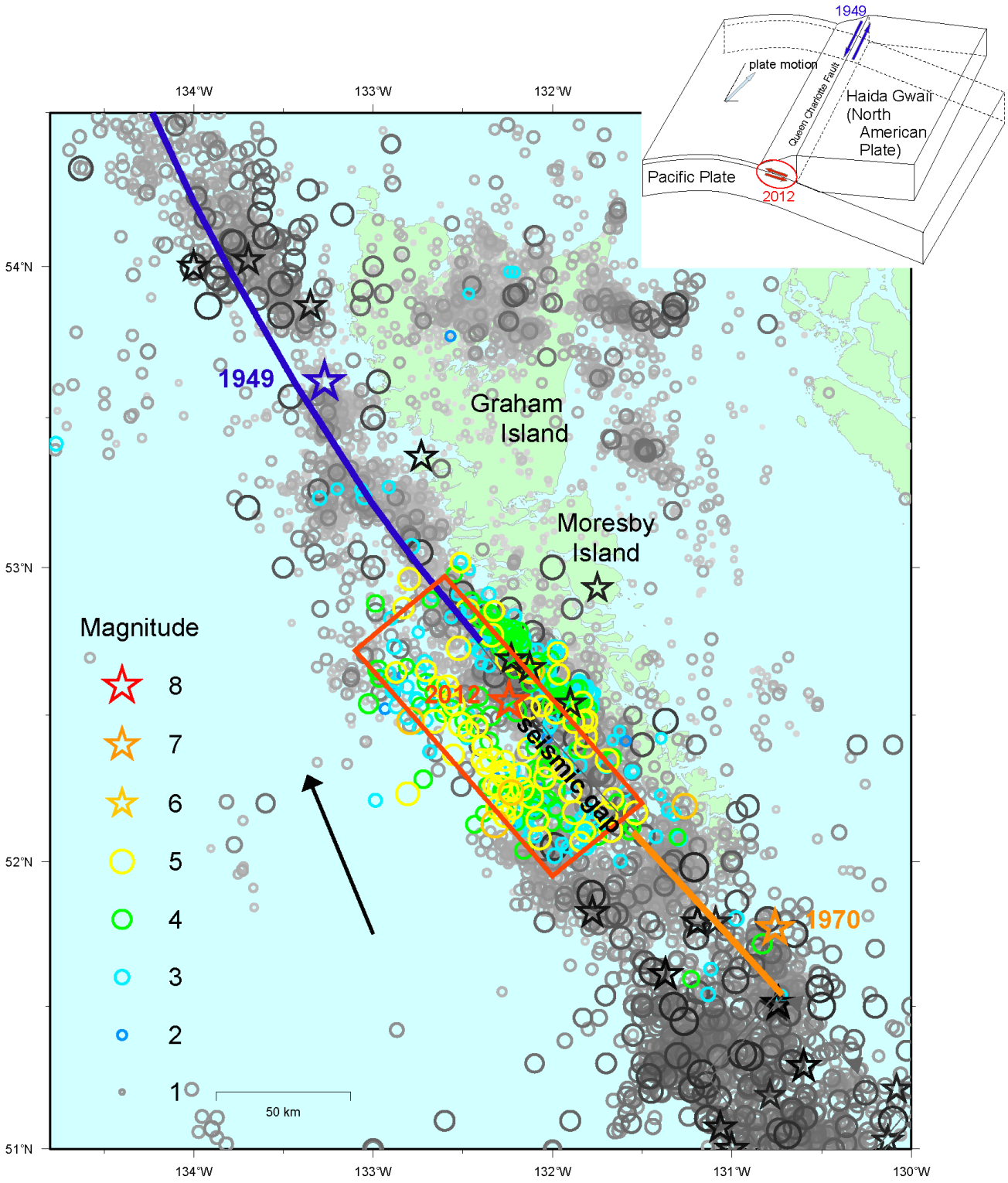

Figure 6.8: *Tectonic setting and historical seismicity (1898 through 2013) of Haida Gwaii, off the coast of British Columbia, with the Queen Charlotte Fault marking the transpressional boundary between the Pacific and North American Plates; the arrow indicates Pacific Plate motion, at roughly 50 mm/y, relative to the North American Plate (from Bird and Lamontagne, 2015a). The rupture length of the M_W 8.1 earthquake in 1949 is shown in blue and that of the M_W 7.4 event in 1970 in orange; the rupture zone of the 2012 event is boxed in red. With the exception of the 1949 and 1970 mainshocks, seismicity that occurred before the M7.8 in 2012 is indicated in a grey scale. The inset figure is of a simplified fault model (adapted from James et al., 2013) showing thrust faulting beneath the Queen Charlotte Fault, with the 2012 M_W 7.8 thrust event (shown in red) believed to have occurred between the Pacific Plate and the accretionary prism. The 1949 M_S 8.1 ruptured along the transform margin to the north.*

6.2.3 Mainshock of the October 2012 Earthquake Sequence

The magnitude 7.8 earthquake of 27th October 2012 (20:04 Pacific Standard Time) is the second largest instrumentally recorded in Canadian history. It was of a predominantly thrust movement (Kao *et al.*, 2015) on a north-eastward dipping fault, believed to lie directly beneath the QCF (Figure 6.8 inset, adapted from James *et al.*, 2013). While the event occurred in the vicinity of the aforementioned seismic gap, it did not occur on the QCF, and it therefore did not release stress as anticipated along that section of fault. That section of the QCF was instead subjected to increased stress as a result of the M_W 7.8 event (Hobbs *et al.*, 2015a).

The mainshock was felt throughout British Columbia and as far away as the Yukon, Alberta and Montana, roughly 1600 km from the epicentre. Nevertheless, this earthquake resulted in limited damage partly due to the population centres being located at least 80 km from the epicentre and 60 km from the fault rupture. Figure 6.9 shows: a) the shaking recorded at the village of Queen Charlotte, at an epicentral distance of roughly 80 km; and b) the attenuation as seen at three regional strong motion seismic stations. Although there was little visible impact and there were few, minor injuries from this earthquake, many people were significantly traumatised by the experience, and by the numerous aftershocks that were felt throughout the following weeks (Bird and Lamontagne, 2015a).

Ground motion

The weak-motion seismic stations operating on Haida Gwaii at the time of the earthquake were saturated by the shaking. Three strong-motion Internet Accelerographs (IAs) in the region did, however, register the event clearly, to a maximum recorded acceleration of $0.2g$ (20% of gravitational acceleration; Rosenberger *et al.*, 2013; Figure 6.9a) in the village of Queen Charlotte at an epicentral distance of 80 km. Most people on Haida Gwaii are familiar with small-to-moderate earthquakes, and following the October 2012 event described having felt considerable shaking for about half-a-minute, at which point they assumed the shaking would diminish, as it had for earthquakes in the past. The shaking instead became much stronger. The perceivable shaking lasted roughly 1.5 minutes, with very strong shaking for about 30 seconds.

Field surveys

In the weeks following the mainshock, Natural Resources Canada (NRCan) technical crews visited the islands and the offshore region to service the existing network of seismometers and to install seven additional seismometers, seven GPS receivers and fourteen ocean-bottom seismometers (James *et al.*, 2013). The latter deployment was complemented by an airgun seismic survey to examine the structure of the rupture region. The land-based fieldwork was supplemented by surveys to map landslides and by expeditions in search of evidence of tsunami run-up. This fieldwork provided data critical in many of the studies outlined below. The seismic and GPS data gathered in the months to follow would be used to accurately locate the tens of thousands of aftershocks and to measure the coseismic crustal deformation associated with this event and the post-seismic relaxation. At time of printing, only ~2%

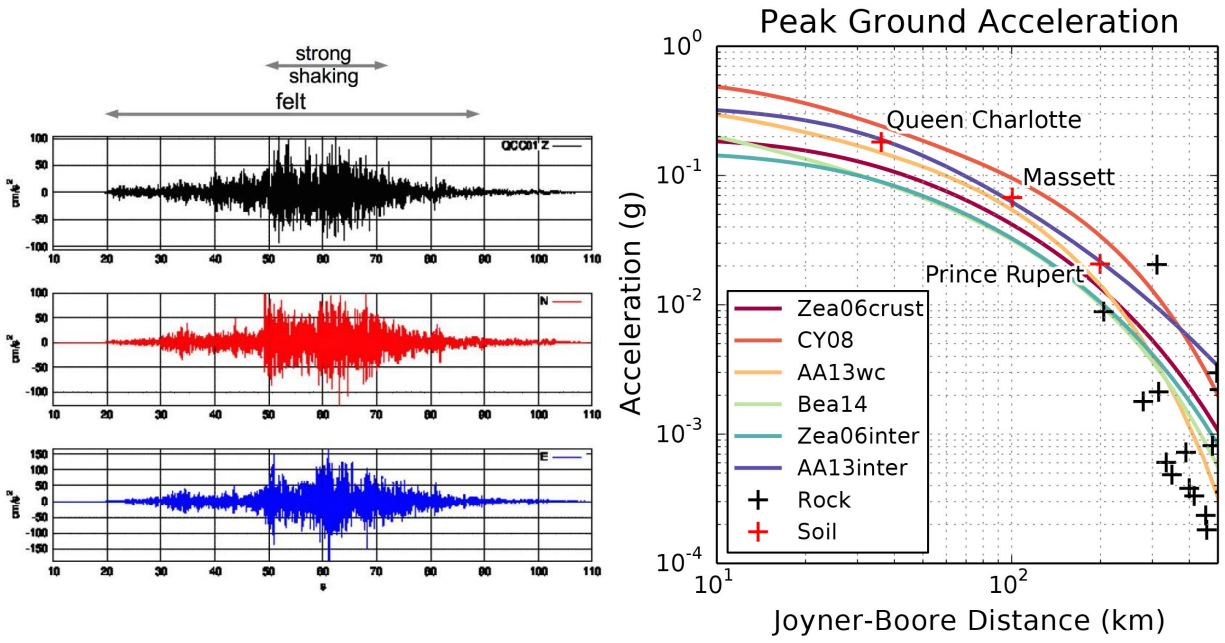

(a) (b)

Figure 6.9:
a) Shaking (acceleration) recorded by the three-component strong-motion Internet Accelerograph at the village of Queen Charlotte, with peak motion up to ~0.2g (~20% gravitational acceleration); this instrument is operated by the Ministry of Transportation and Infrastructure, BC (from Bird and Lamontagne, 2015a).

b) Peak ground acceleration (PGA) recorded at three strong-motion soil sites (red crosses) as well as weak-motion sites on rock (black crosses), shown against well-established ground-motion models for subduction interface environments for an M_W 7.8 earthquake. Ground-motion predictions assume a VS30 of 1,500 m/s appropriate for BC coastal rock sites (Atkinson, 2005). Ground-motion models are shown for subduction interface (Atkinson and Adams, 2013: "AA13inter"; Zhao et al., 2006: Zea06inter) and crustal (Atkinson and Adams, 2013: "AA13wc"; Akkar et al., 2014: "Aea14"; Zhao et al., 2006: Zea06crust) models (after Allen and Brillon, 2015).

of the approximately 100,000 recorded aftershocks have been located by analysts, although automated locations have been acquired for roughly 60%.

Spatiotemporal distribution of events during the first week of aftershocks

Farahbod and Kao (2015) systematically relocated 1229 aftershocks (M_L 1.4 – 5.8) that occurred during the first week of the 2012 Haida Gwaii aftershock sequence by re-examining continuous seismic waveforms of the Canadian National Seismograph Network (CNSN). These efforts primarily benefited from the data recorded at seven stations operated by the CNSN on Haida Gwaii. Whenever corresponding arrivals could be identified, waveforms from other nearby stations in the region were also included to maximise the data constraint. The key principle of the strategy to increase location accuracy is to extract as much information as possible from existing waveforms (Roberts *et al.*, 1989; Ottemöller *et al.*, 2012). In this regard, travel-time differences between P and S phases from at least the three closest stations were measured. Through this process, the presence of numerous micro-aftershocks were revealed in the recordings from the closest station (BNB; Figure 6.10); phases from these micro-events were often wrongly associated by the automatic location routine with phases at neighbouring stations from other

events, resulting in significantly incorrect locations. Thus, it was necessary to carefully re-examine all waveforms to eliminate possible incorrect phase associations due to micro-aftershocks. Finally, back-azimuth information from the closest three-component station was included in the analysis.

Results from these aftershock relocations effectively doubled the size of the CNSN routine earthquake catalogue. The corresponding root-mean-square (RMS) time residual was 0.6 s or less. The distribution of aftershocks formed two linear trends roughly parallel to the strike of the plate margin in the NW–SE direction (Figure 6.10). The band located up-dip from the mainshock within the subducting Pacific plate appears to have three clusters spanning a lateral distance of ∼80 km. The other band is distributed along the surface trace of the QCF. The apparent lack of seismicity along the southern part of the QCF in the source region suggests that the accumulated stress along the QCF was only partially released during the 2012 Haida Gwaii earthquake. The projected hypocentre of the mainshock coincides well with the inferred location of the interplate thrust zone at the ∼16 km depth near the bottom of the seismogenic (locked) zone (Profile A1–A2, Figure 6.11). The overall area of aftershock distribution is ∼120 km by ∼40 km, which overlaps the southern part of the estimated rupture zone of the 1949 M 8.1 Queen Charlotte earthquake (Rogers, 1986; Cassidy *et al.*, 2014).

6.2.4 Physical Impacts

Landslides, debris flows and rock falls were noted by many inhabitants in late-October and November 2012. Several were catalogued by Parks Canada officers and Natural Resources Canada field crews in the weeks following the earthquake as they travelled over the largely uninhabited Moresby Island (e.g., Leonard and Bednarski, 2015). As there was only one helicopter available on the islands and the weather in the months following the mainshock was generally too poor for flight safety, the opportunity to conduct aerial field surveys was extremely limited. Dedicated landslide surveys were, however, conducted by the BC Ministry of Forests, Lands and Natural Resource Operations (Millard, 2012; Millard *et al.*, 2012) and by the Gowgaia Institute (Gowgaia Institute, personal communication, 2012). Numerous slides were documented along the slopes of the islands (Figure 6.12): nearly 100 by the provincial government and many more by the Gowgaia Institute, whose efforts focused on a small area between Gowgaia Bay and Upper Victoria Lake within the Gwaii Haanas National Park.

The thermal springs in Gwaii Haanas National Park having become dry in the wake of the earthquake was a great disappointment to the people of Haida Gwaii. The hot springs' pools were a draw to the kayak and boat visitors to Gwaii Haanas, but they are also a sacred site of the Haida Nation. It is not unusual, however, for water levels in geothermal springs and wells to change height as a result of stress perturbations within the crust, such as for earthquakes (Hurwitz *et al.*, 2014; Husen *et al.*, 2004; Hutchinson, 1985; Rinehart, 1972). No such effects on the Gwaii Haanas hot springs were recorded after the more distant 1949, M_W 8.1 event. It should be noted that within a year some thermal spring activity was detected in the area (CBC, 2014) and in 2015 the springs showed signs of returning (Council of the Haida Nation, 2015).

Shaking from the mainshock caused slumping of the roadway between Port Clements and Masset; although not threatening the pavement itself, the supporting berm failed almost completely in one area. Building damage was generally light and locally variable; physical effects of the shaking on construction

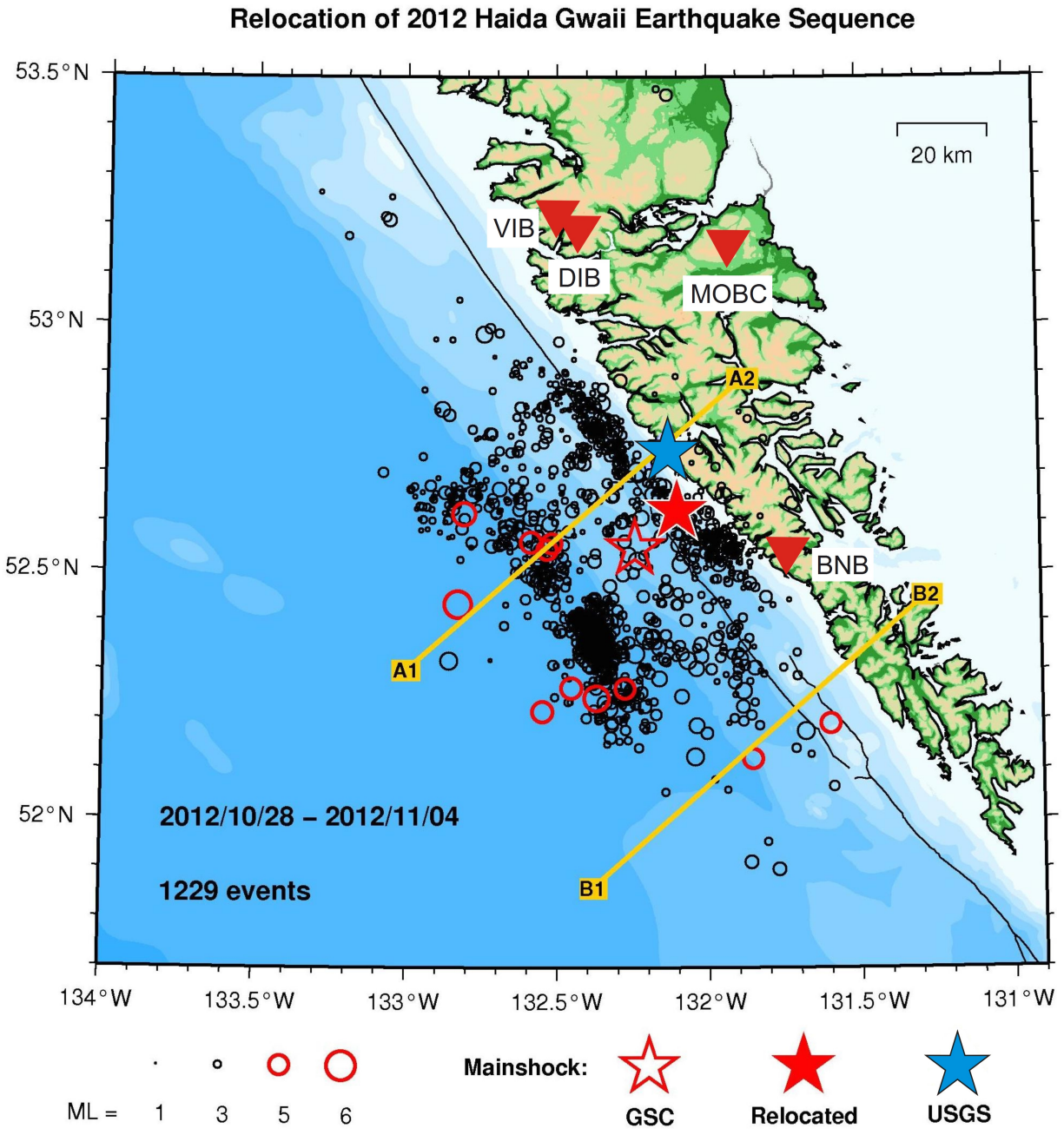

Figure 6.10: *Epicentral distribution of the 2012 Haida Gwaii earthquake sequence (adopted from Farahbod & Kao, 2015). Re-analysed aftershocks that occurred during the first week are indicated by black open circles. Mainshock epicentres are shown by stars: the red and blue solid stars correspond to our relocated result and the US Geological Survey (USGS) report, respectively; the red open star corresponds to the location reported by the Geological Survey of Canada (GSC). Triangles indicate the closest seismic stations. Cross-sections along the two profiles (A1-A2 and B1-B2) are shown in Figure 6.11.*

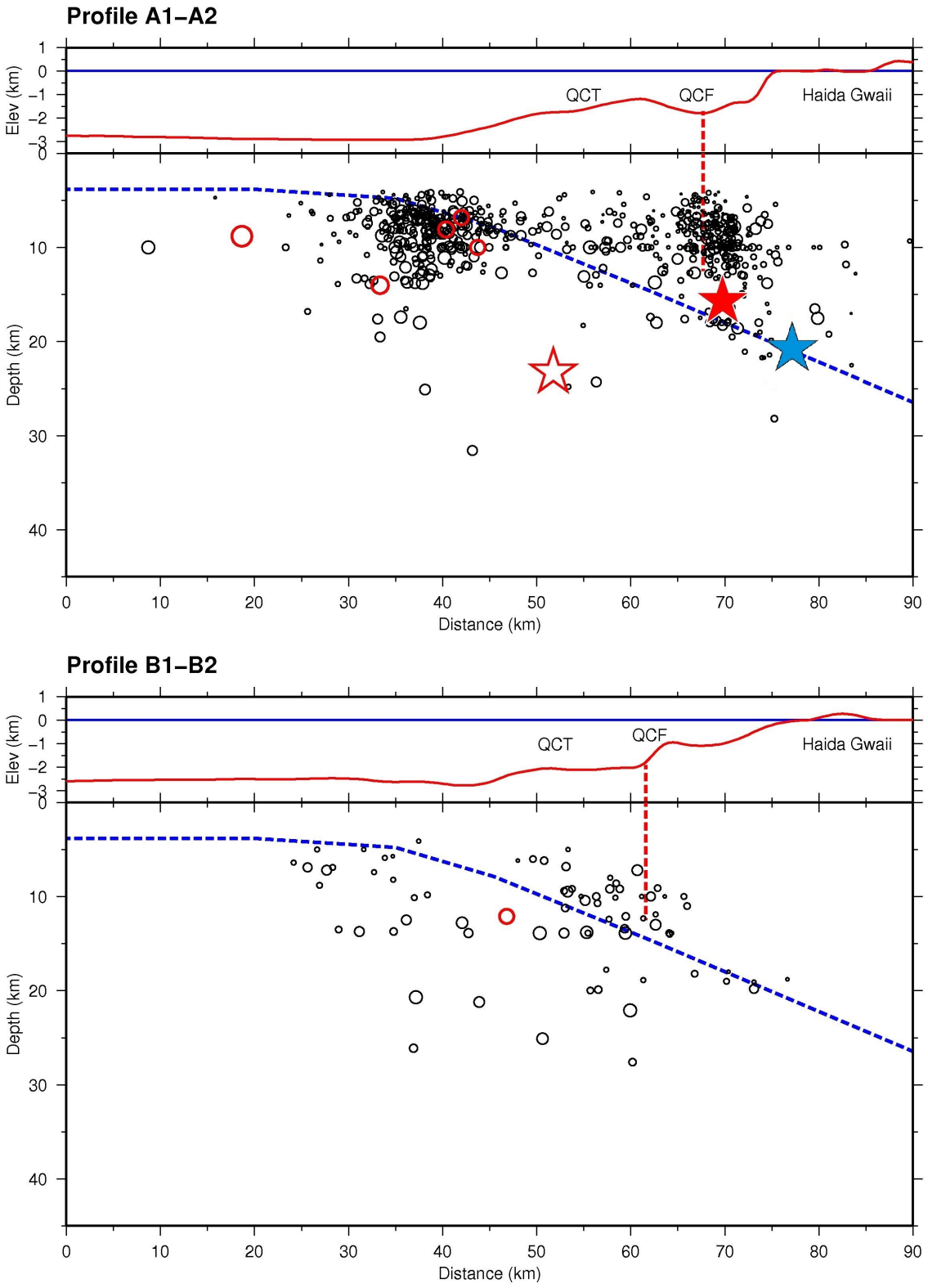

Figure 6.11: *Depth distribution of the 2012 Haida Gwaii earthquake sequence along two cross-sections (adopted from Farahbod and Kao, 2015). Geographic locations of the two profiles are marked in Figure 6.10. Events within 25 km from each side of the profiles are projected onto a vertical plane. Stars represent the projected hypocentres of the mainshock (red and blue solid stars are for relocated results of Farahbod and Kao (2015) and the USGS report, respectively; the red open star is the location reported by the GSC). The vertical dashed line marks the approximate location of the QCF. QCT indicates the location of the Queen Charlotte Terrace.*

Figure 6.12: *Map showing locations of geological observations (from Bird and Lamontagne, 2015a), including a rock-fall, indicated by a green triangle (#1: D. Gould) and other landslides (#2: I. Gould ; #3: M. Schmidt; #4: J. Reggler), indicated by red stars or red curves. Landslide surveys were conducted by the BC Ministry of Forests, Lands and Natural Resource Operations (red boxes) and by the Gowgaia Institute (turquoise box). The dried-up thermal springs at Hotspring Island are indicated by the blue diamond (#5: B. Schofield).*

consisted primarily of chimney damage, with a small number of failed chimneys documented as far away as Tlell (115 km from fault rupture), and minor cracks in foundations and walls (Figure 6.13). In contrast, chimney and other building damage was prevalent throughout the islands in the wake of the larger and generally closer, 1949 (M_W 8.1) earthquake, after which only one chimney on the islands is rumoured to have remained standing (Sergis Debussy, personal communication, 2012). Despite the strong shaking experienced on the islands ($\sim$0.2g), many objects in precarious positions were not damaged or displaced. The Queen Bee Café in the village of Queen Charlotte has numerous tall, thin bottles of syrup on a shelf barely wide enough to hold them but none seemed to have moved, yet the entire contents of refrigerators and china cabinets were emptied onto floors in the neighbouring village of Skidegate. It is likely some of the local variations in shaking effects are due to differences in site conditions; all the communities are located close to the water, with sites varying from bedrock to poorly consolidated sediments. Also, while most buildings are of low, wood-frame construction, other structural elements, such as foundations and reinforcement, vary considerably.

6.2.5 Community Decimal Intensities

A combined total of 3,005 reports were submitted to the "Did you feel it?"(DYFI) section of the Geological Survey of Canada (GSC) and United States Geological Survey (USGS) web sites. For each report, a Community Decimal Intensity (CDI; Wald *et al.*, 2011; Dengler and Dewey, 1998) was calculated – details can be found in Bird and Lamontagne (2015a).

Of the DYFI reports, a total of 88 were submitted by the people of Haida Gwaii, representing only about 2% of the population for that time of year. Additionally, the islands lie roughly 100 km from the mainland coast. This results in the intensity data close to the event's epicentre being relatively sparse. The Haida Gwaii dataset was, however, somewhat augmented by information gathered by Bird in November 2012 and February 2014. Regional CDI measurements from individual reports can be seen on Figure 6.13. Further details can be found in Bird and Lamontagne (2015a,b).

ShakeMap for the October 2012 M_W 7.8 Haida Gwaii Earthquake

Following the M_W 7.8 Haida Gwaii earthquake in 2012, a ShakeMap of the event was produced by the U.S. Geological Survey (USGS) through the Global ShakeMap system (Wald *et al.*, 1999; 2006), augmented with macroseismic intensity data from the USGS "Did You Feel It?" system (Wald *et al.*, 1999 and 2011; Worden *et al.*, 2010; Figure 6.14). The ground motions in this representation were calculated relative to a point-source rupture using an approach defined by the Electric Power Research Institute (2003), whereby a distance adjustment is determined for cases where the rupture orientation is assumed to be uniformly distributed in azimuth for combinations of strike-slip and dip-slip ruptures (Allen *et al.*, 2008).

Several extended-source fault-models for this event have since been developed (e.g., Lay *et al.*, 2013), allowing for an updated ShakeMap for the 2012 earthquake. The Lay *et al.* (2013) fault model was used as the source for calculating closest distance to rupture for the ground-motion calculations. Additionally, DYFI data from the USGS and NRCan on-line systems, along with field reconnaissance reports (Bird and Lamontagne, 2015a), were employed.

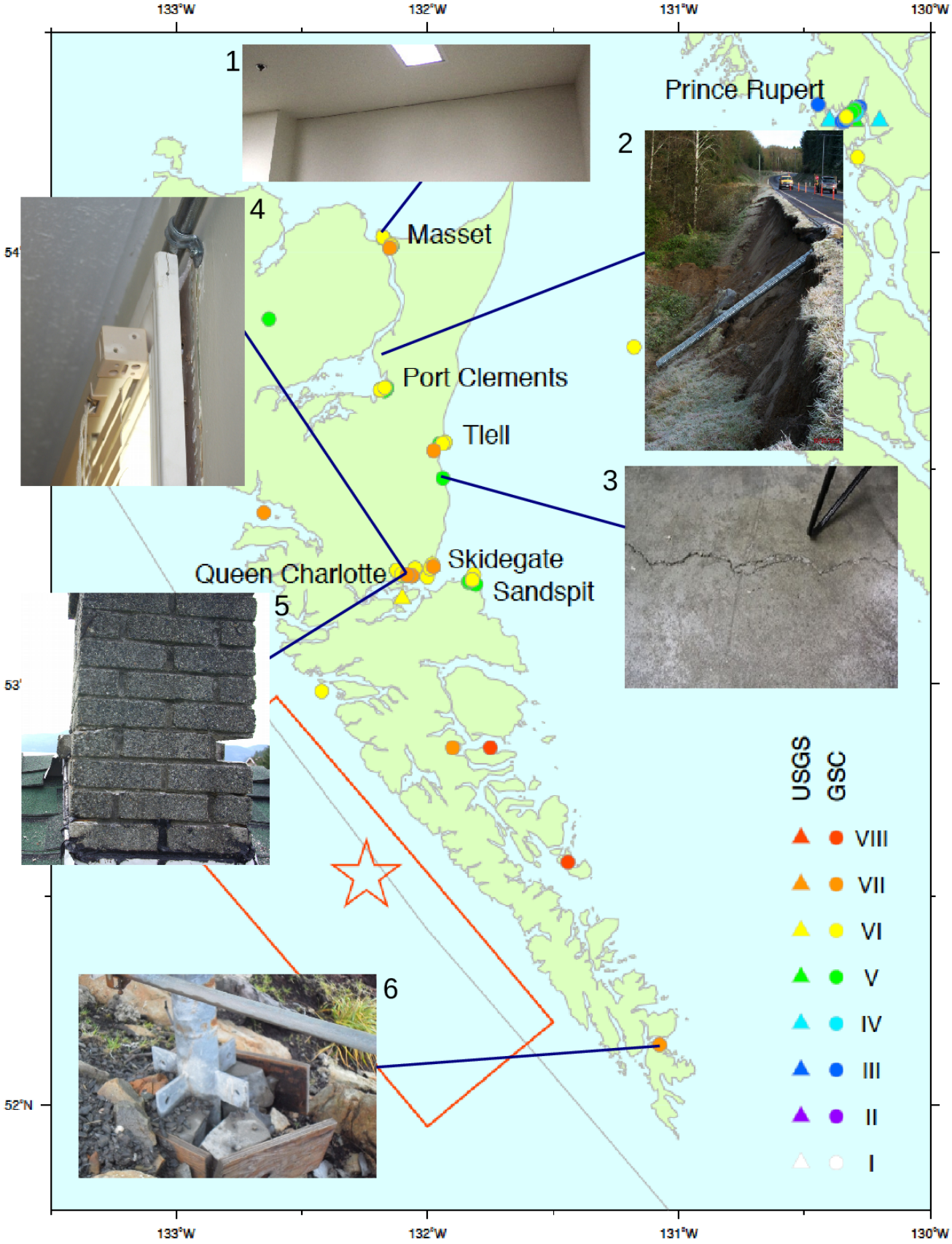

Figure 6.13: *Close-up map of individual intensities (from Bird and Lamontagne, 2015a), together with a selection of images of damage: wall-ceiling separation (#1: A. Bird), road slump (#2: A. Cober), cracked slab (#3: A. Bird), trim separation (#4: J. Goetzinger), chimney damage (#5: J. Goetzinger), and support-strut failure (#6: Canadian Coast Guard).*

Allen and Brillon (in press) found that no one ground-motion model (GMM) adequately captured all characteristics of ground-motion attenuation in the Haida Gwaii region. Zhao *et al.* (2006) was determined to be the most appropriate GMM for this event and was used in the development of the updated ShakeMap. The map (Figure 6.15) includes the effects of site response based on the topographic slope method (Wald and Allen, 2007). The PGV (Peak Ground Velocity) was subsequently converted to macroseismic intensity using the conversion equation of Worden *et al.* (2012) (Figure 6.16). The attenuation of intensity with distance was generally comparable to the assumed model, with the intensity map adjusted by a small inter-event residual of -0.14 macroseismic intensity units (Figure 6.16). The NRCan ShakeMap shows generally higher levels of ground-shaking on Haida Gwaii relative to the USGS ShakeMap. This is primarily due to the inclusion of the extended source model not in the other ShakeMap.

6.2.6 Source Characteristics

Kao *et al.* (2015) systematically determined regional moment-tensor solutions for all significant ($M_L \geq 4$) events in the 2012 Haida Gwaii earthquake sequence. Three-component waveforms from broadband stations of the CNSN at regional distances ($\leq$1500 km) were retrieved for each event. Waveform data from broadband stations in the neighbouring states (Alaska and Washington) were also obtained from the Data Management Center of the Incorporated Research Institutions for Seismology (IRIS DMC) to further improve the azimuthal coverage. The moment-tensor inversion was solved by singular value decomposition of a linear system consisting of observed waveforms and Green's functions of synthetic seismograms, as described in detail by Kao *et al.* (2012).

The focal mechanism of the M_W 7.8 mainshock shows low-angle thrust faulting along a shallowly dipping plane with a strike parallel to the QCF, consistent with the inference of Pacific Plate under-thrusting beneath the overriding North American Plate (Figure 6.17). The results clearly indicate that many seismogenic structures were involved in the 2012 Haida Gwaii earthquake sequence (Figures 6.18 and 6.19). The majority of significant aftershocks show normal-faulting mechanisms that are probably associated with the bending stress within the Pacific plate near the deformation front. Several normal and strike-slip events at greater depths within the subducted Pacific slab show a consistent pattern of T-axis in the down-dip direction, implying that the subducted plate is under a stress regime of down-dip extension. The forearc region is also in extension, but only a few strike-slip events are located along the QCF. The limited size and distribution of the strike-slip events along the QCF suggest that most of the accumulated elastic strain was not released during the 2012 Haida Gwaii sequence. The likelihood of having major strike-slip earthquakes along the southernmost part of the QCF system in the future cannot be ignored.

6.2.7 Coulomb Stress Studies and Overall Rupture Characteristics

Hobbs *et al.* (2015a) studied potential stress triggering resulting from the Haida Gwaii M_W 7.8 mainshock by comparing predicted Coulomb stress changes with the location and mechanism of aftershocks. In addition, they investigated Coulomb stress changes on the nearby Queen Charlotte Transform Fault (Figure 6.20). Using existing rupture models, a high proportion of aftershocks (large and small) were

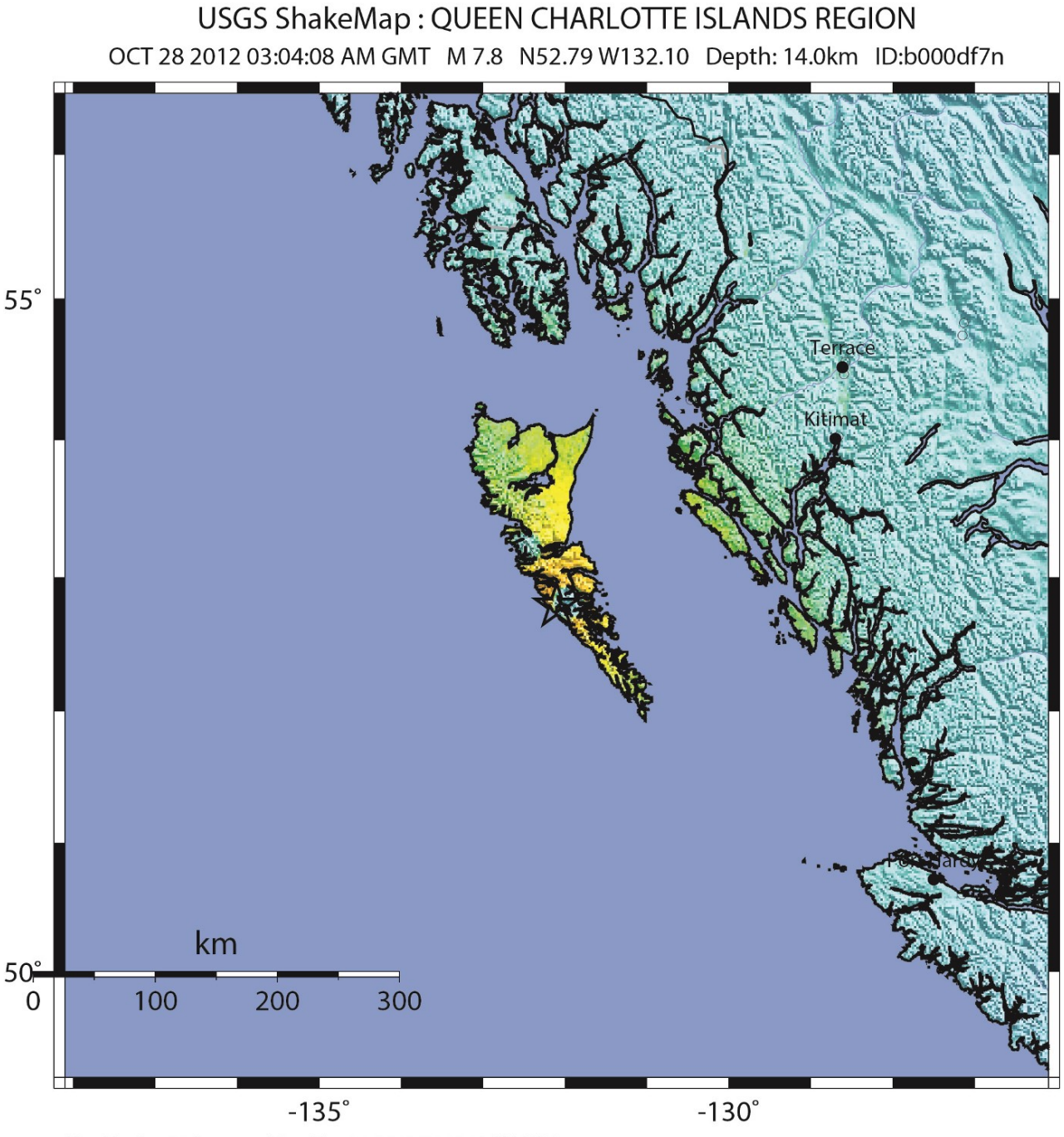

PERCEIVED SHAKING	Not felt	Weak	Light	Moderate	Strong	Very strong	Severe	Violent	Extreme
POTENTIAL DAMAGE	none	none	none	Very light	Light	Moderate	Mod./Heavy	Heavy	Very Heavy
PEAK ACC.(%g)	<0.05	0.3	2.8	6.2	12	22	40	75	>139
PEAK VEL.(cm/s)	<0.02	0.1	1.4	4.7	9.6	20	41	86	>178
INSTRUMENTAL INTENSITY	I	II-III	IV	V	VI	VII	VIII	IX	X+

Scale based upon Worden et al. (2011)

Figure 6.14: *USGS ShakeMap showing the earthquake epicentre (black star). The base shaking was determined through combining the Chiou and Youngs (2008) ground-motion model with the Worden et al. (2012) ground-motion-to-intensity conversion equation (Source:* `http://earthquake.usgs.gov/earthquakes/shakemap/global/shake/b000df7n/` *).*

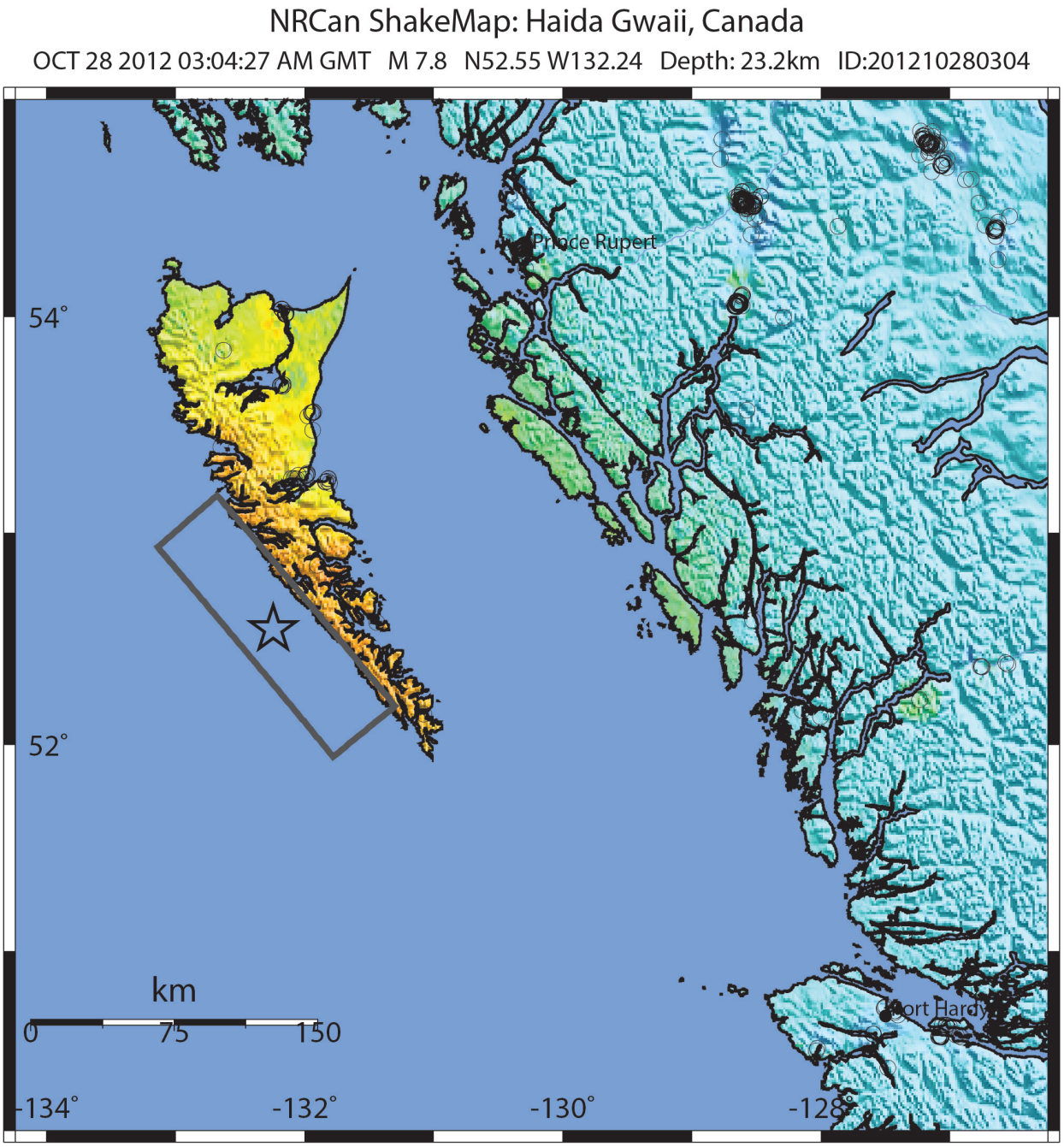

PERCEIVED SHAKING	Not felt	Weak	Light	Moderate	Strong	Very strong	Severe	Violent	Extreme
POTENTIAL DAMAGE	none	none	none	Very light	Light	Moderate	Mod./Heavy	Heavy	Very Heavy
PEAK ACC.(%g)	<0.05	0.3	2.8	6.2	12	22	40	75	>139
PEAK VEL.(cm/s)	<0.02	0.1	1.4	4.7	9.6	20	41	86	>178
INSTRUMENTAL INTENSITY	I	II-III	IV	V	VI	VII	VIII	IX	X+

Scale based upon Worden et al. (2011)

Figure 6.15: *NRCan ShakeMap showing the earthquake epicentre (black star) and the surface projection of the extended fault model of Lay et al. (2013; black polygon). The base shaking was determined through combining the Zhao et al. (2006) ground-motion model with the Worden et al. (2012) ground-motion-to-intensity conversion equation. Open grey circles indicate sites from which a DYFI report was submitted.*

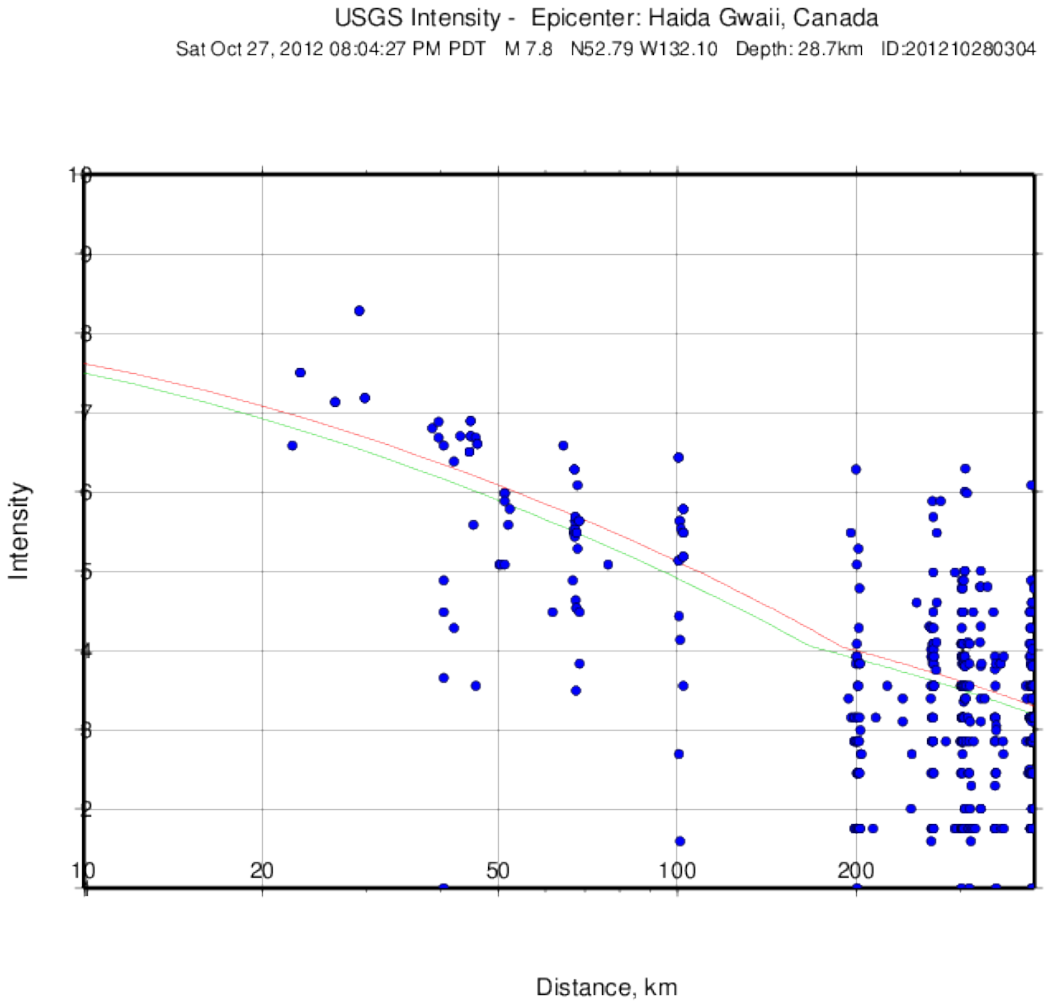

Figure 6.16: *The modelled macroseismic intensity attenuation curve (red line) superimposed by the intensity observations (filled blue circles). The green line indicates the attenuation curve adjusted by the inter-event intensity residual.*

found to be consistent with triggering by the mainshock Coulomb stress changes. For example, up to 86% of all $M_W \geq 4.5$ aftershocks had at least one nodal plane that was positively stressed. Additionally the observed cluster of aftershocks seaward of the main thrust falls within the modelled zone of promoted normal failure, likely related to extension in the footwall. Further, Hobbs *et al.* (2015a) found loading greater than the triggering threshold on nearby portions of the Queen Charlotte Fault, in particular the region to the south of the 2012 mainshock (Figure 6.20b). This segment of the Queen Charlotte Fault was identified (Rogers 1986) as a seismic gap with the potential for an event as large as M 7.5. With increased stress loading from the 2012 earthquake, this suggests increased seismic hazard in the region.

Hobbs *et al.* (2015b) used global Rayleigh and Love wave recordings of the M_W 7.8 mainshock with an Empirical Greens Function (EGF) deconvolution technique (using a nearby well-recorded M_W 6.3 thrust event as the EGF) to determine Relative Source Time Functions (RSTFs) that yield information on the overall rupture characteristics of the mainshock. Resulting RSTFs commonly displayed two peaks, confirming the presence of two dominant sub-events. This was suggested originally by Hayes (2013) and Lay *et al.* (2013).

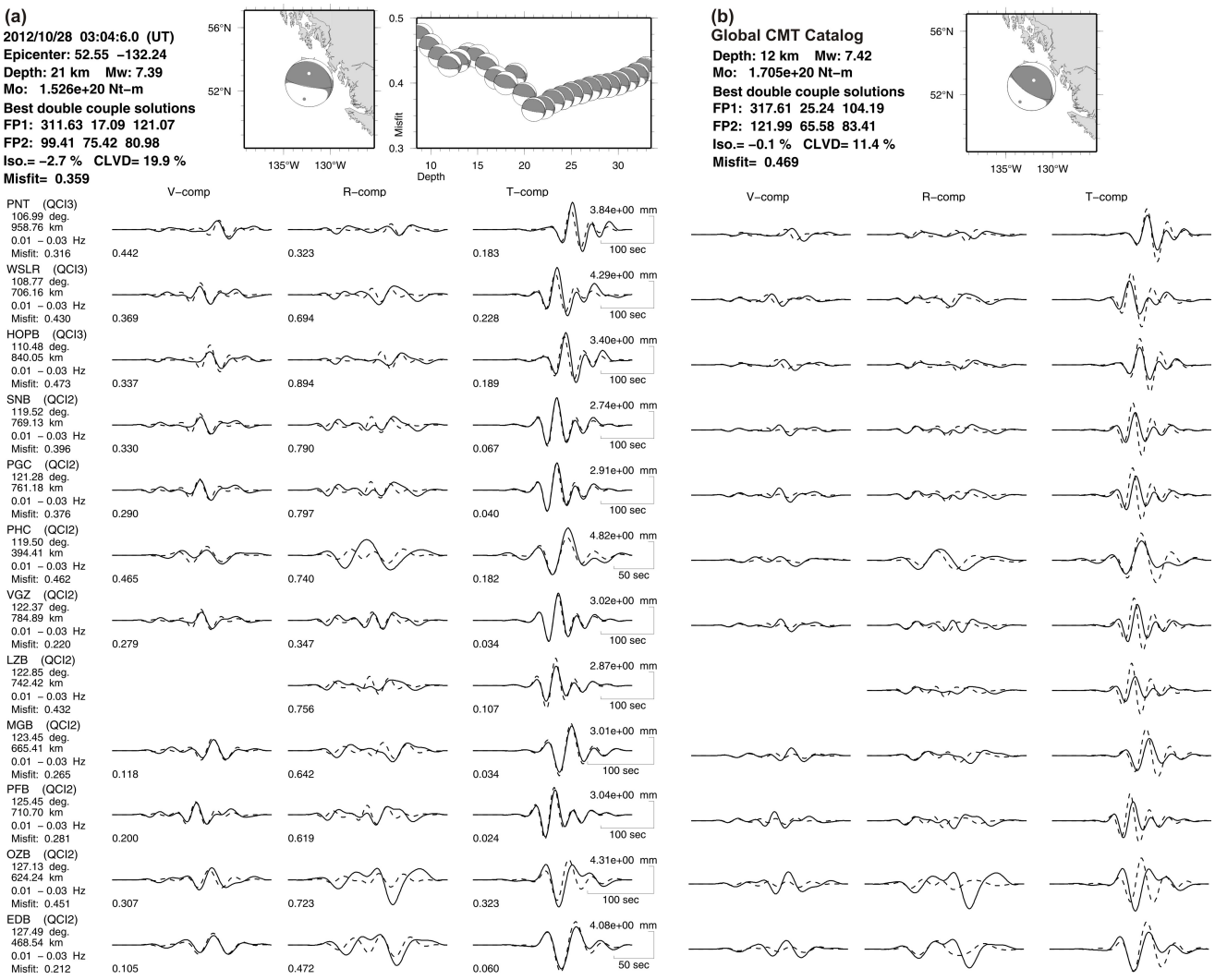

Figure 6.17: *Moment-tensor inversion result for the 2012 Haida Gwaii earthquake mainshock (adopted from Kao et al., 2015). (a) Source parameters are summarised on the top with a map showing the epicentral location and the focal mechanism. The best-fitting depth is 21 km, as shown by the misfit vs depth curve. Observed and synthetic waveforms for each station are plotted as solid and dashed lines, respectively. Waveform misfit of each component is listed at the lower-left corner of each trace and the station average is shown on the left. Kao et al.'s solution has a minor strike-slip component that is compatible with the relative plate motion. Overall the waveform fit is excellent. (b) Results of forward modelling based on the solution reported in the Global CMT Project database. The waveform fit is clearly not as satisfactory.*

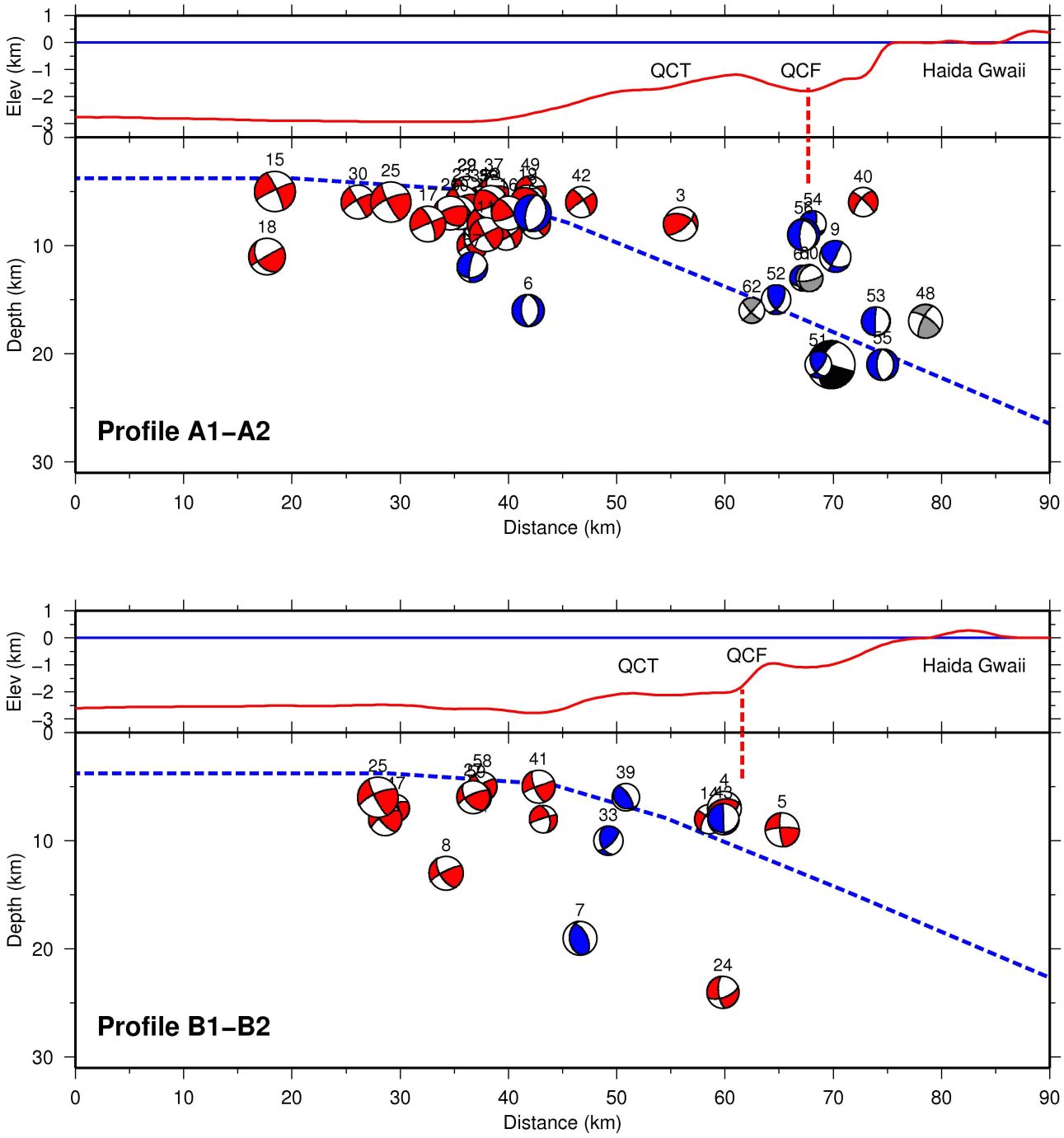

Figure 6.18: *Vertical profiles showing the hypocentral distribution and focal mechanisms (in back-hemisphere projection) of significant aftershocks in the 2012 Haida Gwaii earthquake sequence (adapted from Kao et al., 2015). Different colours/shadings correspond to different types of faulting (red: normal-faulting; blue: strike-slip faulting; grey: thrust-faulting). The mainshock is plotted in black. Local bathymetry and topography are plotted at the top of each profile. Dashed blue and red lines mark the top of the under-thrusting Pacific plate and the Queen Charlotte Fault (QCF), respectively. QCT denotes the Queen Charlotte Terrace. Vertical exaggeration of the bathymetry/topography is 2.5. Geographic locations of the two profiles are available in Figure 6.10.*

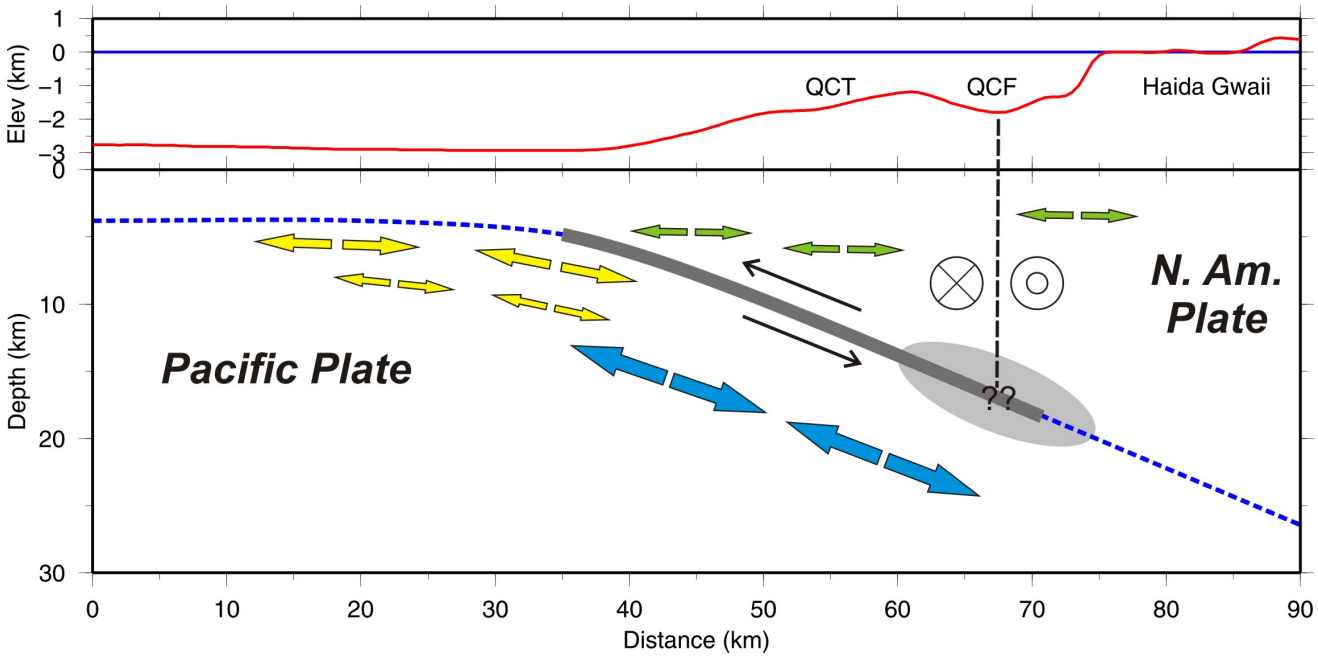

Figure 6.19: *A schematic diagram summarising the seismogenic structures of the 2012 Haida Gwaii earthquake sequence. The layout is similar to that in Figure 6.18 with symbols representing the Queen Charlotte Fault (QCF, vertical dashed line) and the rupture zone of the mainshock (thick dark line). A pair of black arrows represents the relative plate motion along the interface; target signs on the two sides of the QCF symbolise the dextral shear motion across the fault zone. Pairs of arrows near the deformation front correspond to the extensional stress regime due to plate bending. Pairs of arrows beneath the Queen Charlotte Terrace (QCT) and Haida Gwaii indicate the existence of extension within the overriding North America crust. Large arrows symbolise the stress regime of down-dip extension within the down-going Pacific plate. The grey area marks the location where complex interactions between the QCF and the interplate thrust zone might have occurred.*

Overall, Hobbs *et al.* (2015b) found compelling evidence that the 2012 Haida Gwaii earthquake had uneven bilateral overall rupture with a well-resolved component to the northwest (Figure 6.20a). The first, largest sub-event, approximately 14 s after the onset of rupture, was located roughly 12 km to the south of the epicentre. The second sub-event, 17 s after the first sub-event (i.e. ∼31 s after the onset of rupture), was located directly along strike to the northwest at about 28 km from the first sub-event. The overall rupture (from the beginning to end of the RSTFs) migrated a distance of approximately 50 km at 308.5° azimuth and took about 43 s to break. Interestingly, this overall northwest-directed rupture may aid in explaining the observed focusing of surface waves at Alaskan seismic stations (Gomberg, 2013). Future work could examine the potential for delayed-onset dynamic triggering of the Craig, Alaska, earthquake of January 2013 (Gomberg, 2013; Lay *et al.*, 2013) that occurred two months later and ∼300 km to the NW of the 2012 Haida Gwaii mainshock.

6.2.8 GPS Observed Crustal Displacements

A geodetic study of the coseismic and postseismic displacements resulting from this earthquake was carried out by Nykolaishen *et al.* (2015). Global Positioning System (GPS) data collected in the weeks following the event were used along with historical data sets to determine coseismic offsets at sites throughout southern Haida Gwaii. The largest measured offset was 115 cm in a SSW direction, accompanied by 30 cm of subsidence measured at Barry Inlet (Figure 6.21). These offsets are consistent

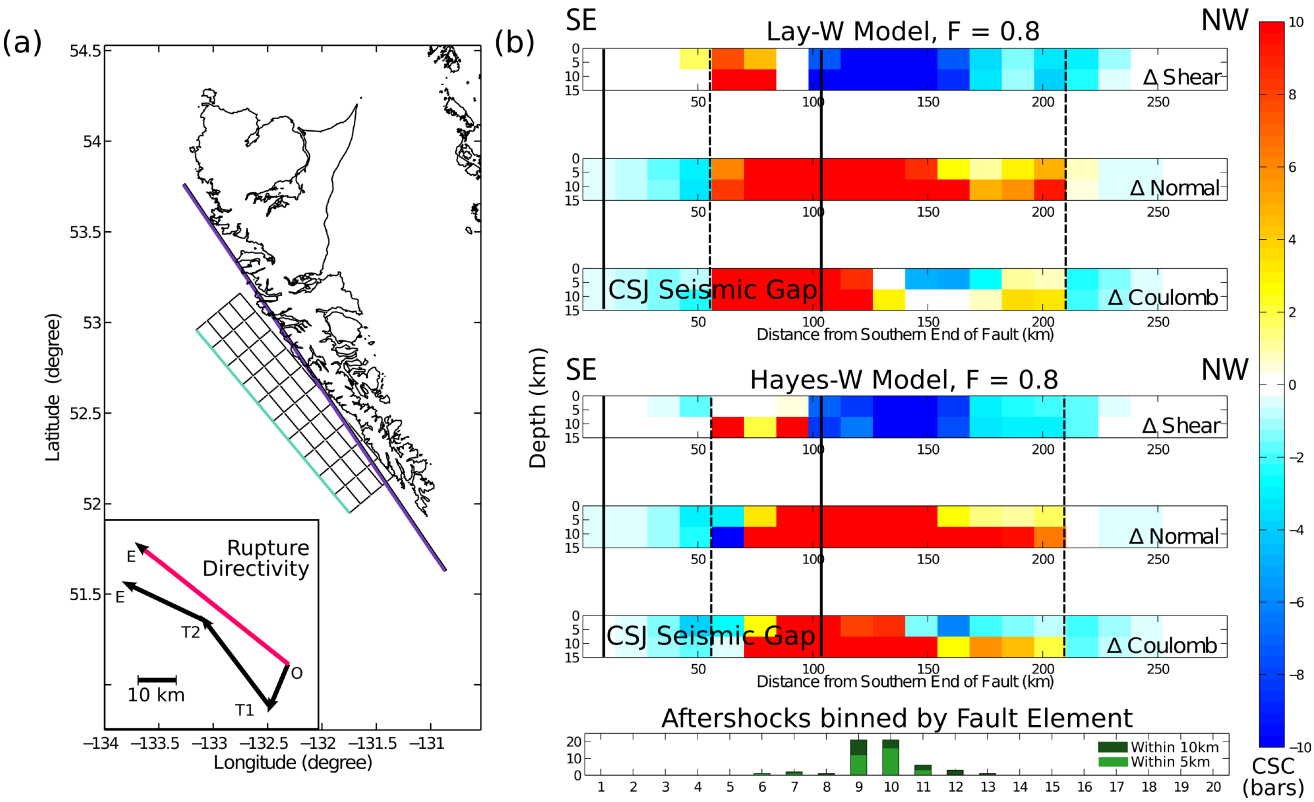

Figure 6.20: *(a) The Haida Gwaii rupture zone (pictured as a fault-element grid with a turquoise surface trace) is considered based on its geometry relative to the Queen Charlotte Fault (purple line). Results of empirical Green's function deconvolution and directivity analysis are inset, with apparent directivity sub-parallel to the Haida Gwaii mainshock's rupture-zone strike and the strike of the Queen Charlotte Fault (from Hobbs et al., 2015b). (b) Shear, normal, and total Coulomb stress changes (CSC), in bars, projected onto the Queen Charlotte Fault, as indicated in (a), using the Lay-W and Hayes-W models and a friction coefficient of 0.8. The extent of the Cape St. James (CSJ) Seismic Gap is indicated at the southern end of the fault. The bottom trace indicates the numbers of aftershocks whose surface projections are within 5 and 10 km, horizontally, of the Queen Charlotte Fault. (from Hobbs et al., 2015a)*

with a shallow dipping thrust beneath the Queen Charlotte Terrace, as identified by static finite-fault rupture models based solely on other observations (seismic/tsunami). These preliminary fault-rupture models, however, do not replicate the magnitudes of GPS-observed horizontal offsets or subsidence throughout the region. Nykolaishen *et al.* (2015) updated selected existing finite-fault models (e.g., Lay *et al.*, 2013) through inversion of the three-component GPS observations and by constraining the rupture to occur offshore Haida Gwaii, in an attempt to replicate the observed subsidence on western Haida Gwaii. Overall, the inversions yielded two important differences compared to the starting models used: (1) the observed subsidence at the Barry Inlet station on the west coast of Haida Gwaii was correctly predicted, and (2) the slip along the fault surface was concentrated at the southern end of the rupture zone (Figure 6.21).

Continued monitoring of displacements resulting from this event has indicated up to 6 cm of cumulative horizontal motion in the first year following the mainshock. These postseismic motions range in direction from south-southwest at stations on northern Moresby Island (similar to the coseismic offsets), to southeast or east-southeast at stations on southern Moresby Island (Figure 6.22). The nature of the postseismic displacements over time are similar to those observed at other subduction zones (e.g., Ozawa *et al.*, 2012; Wang *et al.*, 2012; Sun *et al.*, 2014), with the fastest displacement rate occurring in the

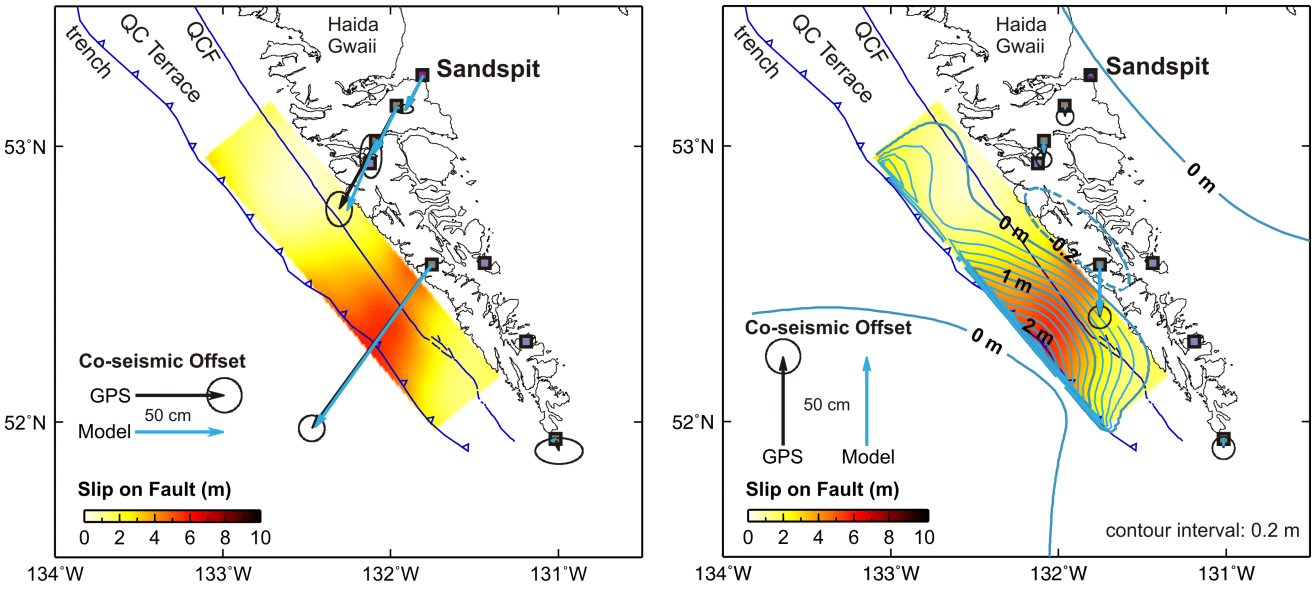

Figure 6.21: *Comparison of observed coseismic offsets (black arrows) at GPS stations on Haida Gwaii to those predicted from non-linear Bayesian inversions of three-component GPS observations (blue arrows) using the finite-fault rupture model of Lay et al. (2013) as the starting model. (Left) Horizontal component of inversion results. Error ellipses represent 95% confidence intervals using standard deviation values five times the values of uncertainties reported in Nykolaishen et al. (2015) for coseismic offsets in the north and east components. (Right) Vertical component of inversion results. The direction of arrows denotes uplift or subsidence and blue contours show the predicted coseismic vertical deformation pattern in southern Haida Gwaii from the inversion. The diameters of the error circles represent 95% confidence intervals using standard deviation values twice the values of uncertainties reported in Nykolaishen et al. (2015) for the vertical coseismic offsets. QCF denotes the Queen Charlotte Fault.*

first few weeks after the earthquake. Preliminary analysis of the time series from the station at Sandspit (Figure 6.21 and 6.22) necessitated fitting a function with multiple decay terms to accommodate this fast displacement rate immediately post-earthquake, along with a slower decay of the postseismic signal over hundreds of days (Nykolaishen *et al.*, 2015).

The spatial variations in the observed postseismic deformation pattern over the GPS network, along with preliminary curve-fitting of postseismic time-series, may indicate that more than one physical process is contributing to the surface deformation. The processes likely include after-slip and viscoelastic stress relaxation, as observed after other subduction zone earthquakes (e.g., Hu and Wang, 2012; Sun *et al.*, 2014). In addition, Nykolaishen *et al.* (2015) suggest that the eastward component of motions observed at the southern stations (Figure 6.22) could indicate a contribution from aseismic slip (creep) along the Queen Charlotte Fault or along sub-parallel faults (Rohr, 2015) offshore southern Moresby Island.

6.2.9 Tsunami

The Haida Gwaii thrust earthquake caused displacement of the seafloor off the west coast of Moresby Island that triggered the largest locally-generated tsunami along the British Columbia coastline documented in written history (the last ~150 years). The tsunami was recorded by tide gauges and Deep-ocean Assessment and Reporting of Tsunamis (DART) buoys throughout the Pacific Ocean, as well as by NEPTUNE Canada bottom-pressure sensors offshore Vancouver Island (Fine *et al.*, 2015). The largest recorded peak-to-trough wave height of 1.52 m occurred at Kahului, Maui, Hawaii, but only 0.52 m

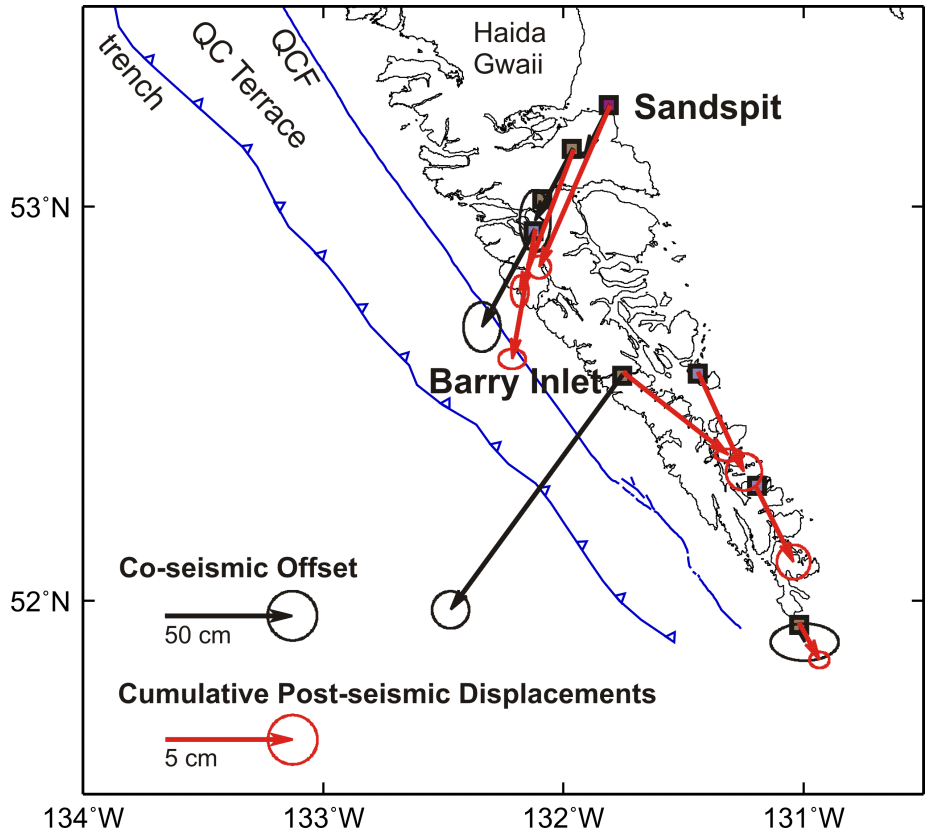

Figure 6.22: *Observed coseismic offsets at GPS stations on Haida Gwaii (black arrows) compared to cumulative postseismic displacements with interseismic deformation signal removed (red arrows). Postseismic displacements were calculated with data available from 28 October 2012 to 31 December 2013. Error ellipses represent 95% confidence interval using standard deviation values five time the values of uncertainties reported in Nykolaishen et al. (2015) for coseismic offsets and cumulative postseismic displacements, respectively, in the north and east components. QCF denotes the Queen Charlotte Fault.*

was recorded at Henslung Cove, Langara Island, off northern Haida Gwaii (Figure 6.23; NGDC/WDS Global Historical Tsunami Database, 2013). Larger waves were, however, expected to have occurred on the unpopulated, non-instrumented west coast of Moresby Island.

Three field surveys in November 2012, February 2013 and June 2013 documented evidence that tsunami run-up exceeded 3 m above the state of tide at the time of the tsunami at sites spanning ~230 km of the western Haida Gwaii coastline (Figure 6.23; details in Leonard and Bednarski, 2014). Greatest impacts were apparent at the heads of narrow inlets and bays on western Moresby Island, where natural and man-made debris with a clear ocean-ward origin was found on the forest floor and caught in tree branches, inferring flow depths and run-up heights of up to 2.5 m and 13 m, respectively (Figures 6.23 and 6.24). Logs disturbed from their apparent former footprints on the forest floor at the head of Pocket Inlet (Figure 6.24) provided evidence of complex tsunami run-up, backwash and oblique flow patterns. Discontinuous muddy sediments were found at a few sites, but the thickness of deposits was not proportional to run-up. Given the limited sedimentological signature of the Haida Gwaii tsunami and evidence for long-term uplift of this coastline (e.g., Clague *et al.*, 1982), it is likely that evidence of the tsunami has a very low preservation potential (Leonard and Bednarski, 2015).

A numerical tsunami model was initially designed to provide preliminary run-up estimates on the west coast of Moresby Island and was used as an aid to the post-tsunami survey teams in 2012 and 2013. The

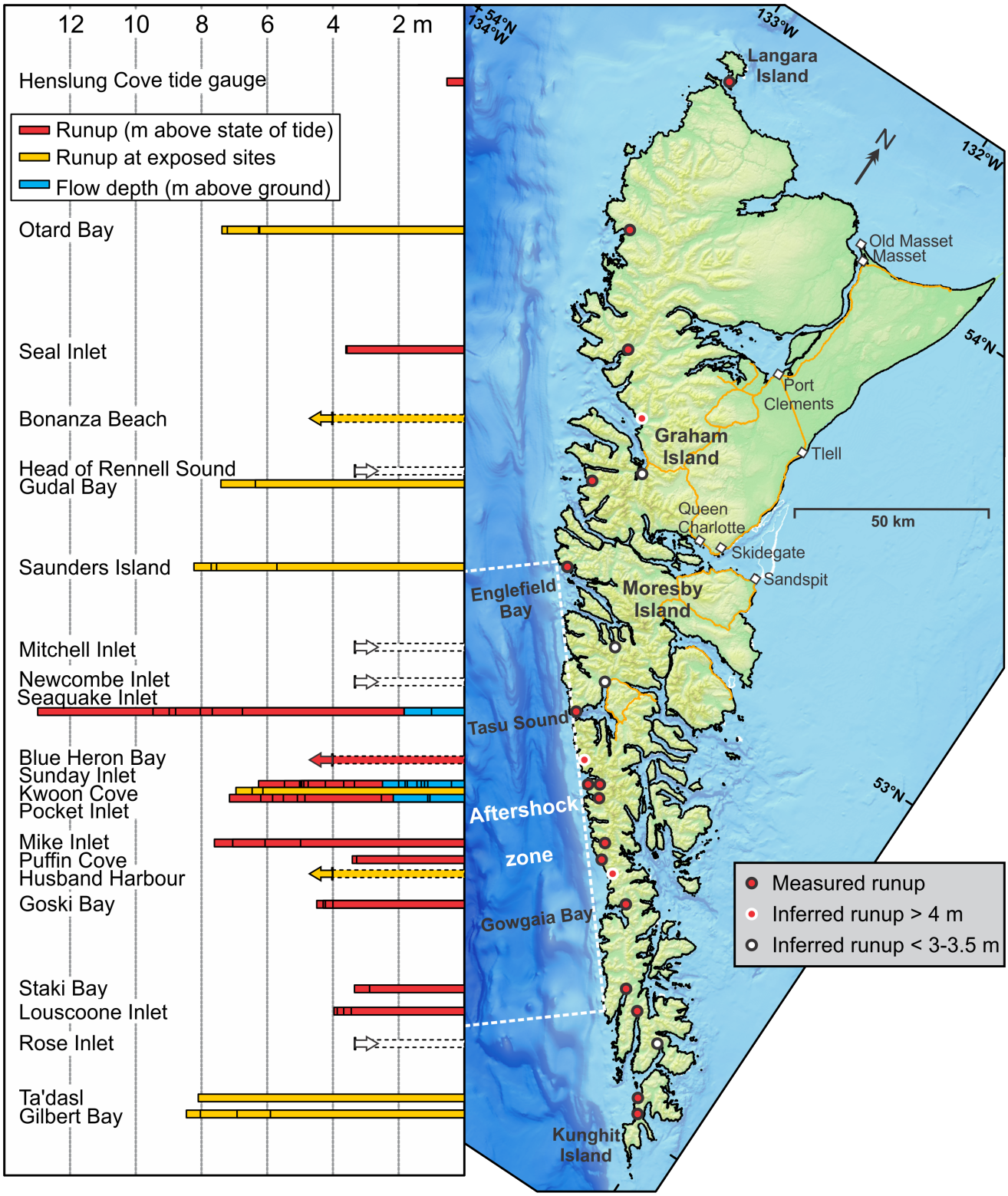

Figure 6.23: *Haida Gwaii survey locations, run-up and flow depth data. Dashed bars indicate inferred minimum/maximum run-up at non-surveyed sites; red/orange indicates that debris was seen to exceed the elevation of the forest edge by at least 1 m; white indicates that debris was not observed to exceed the forest edge elevation. The "run-up" value from Henslung Cove tide gauge is the measured peak-to-trough tsunami amplitude (from Leonard and Bednarski, 2015).*

Figure 6.24: *Tsunami evidence from western Moresby Island (see Figure 6.23 for locations). (a) Variety of debris at Seaquake Inlet. This uncharted inlet has no official name. It was referred to as Davidson Inlet by Leonard and Bednarski (2014) on the basis of its proximity to Davidson Point; the alternative name Seaquake Inlet was proposed by the captain of the CCGS Bartlett following a bathymetric survey of the inlet in August 2013. (b) Fucus seaweed in tree branches at Sunday Inlet. (c) Disturbed logs at Pocket Inlet. (d) Mud deposit at Staki Bay (from Leonard and Bednarski, 2014).*

tsunami source in the more recent version of this model (Fine *et al.*, 2015) was based on the updated finite-fault model of Hayes (2013). To match the tsunami wave arrival-times observed in the DART data, the source region was shifted in the model about 30 km to the southeast. The model-simulated tsunami run-up exceeded 6 m in many places along the coast (Figure 6.25), in good agreement with the post-tsunami surveys (Figure 6.26). This comparison was, however, limited to the bays that are well sheltered from storm-generated waves. Thus the maximum modelled elevation of about 9 m (Figure 6.26) was in a small open bay that has not been surveyed. Furthermore, the largest run-up of 13 m found by the post-tsunami survey team was in a small semi-sheltered inlet just north of Tasu Sound. This large run-up value is not reproduced in the models, a discrepancy that is still under investigation.

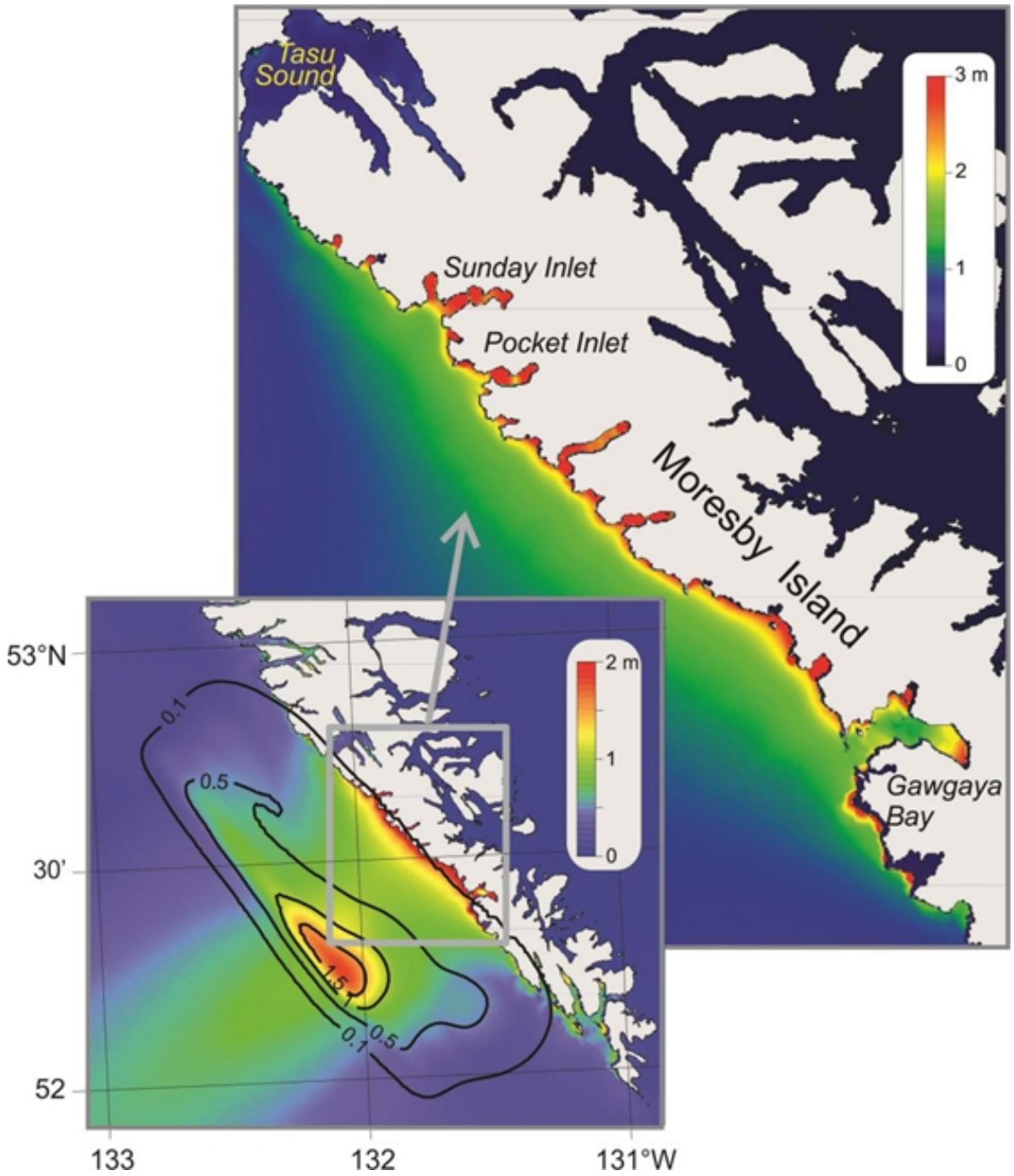

Figure 6.25: *Maximum modelled tsunami elevations off the west coast of Moresby Island. The inset also shows the contours of the initial sea surface uplift (modified from Fine et al., 2015).*

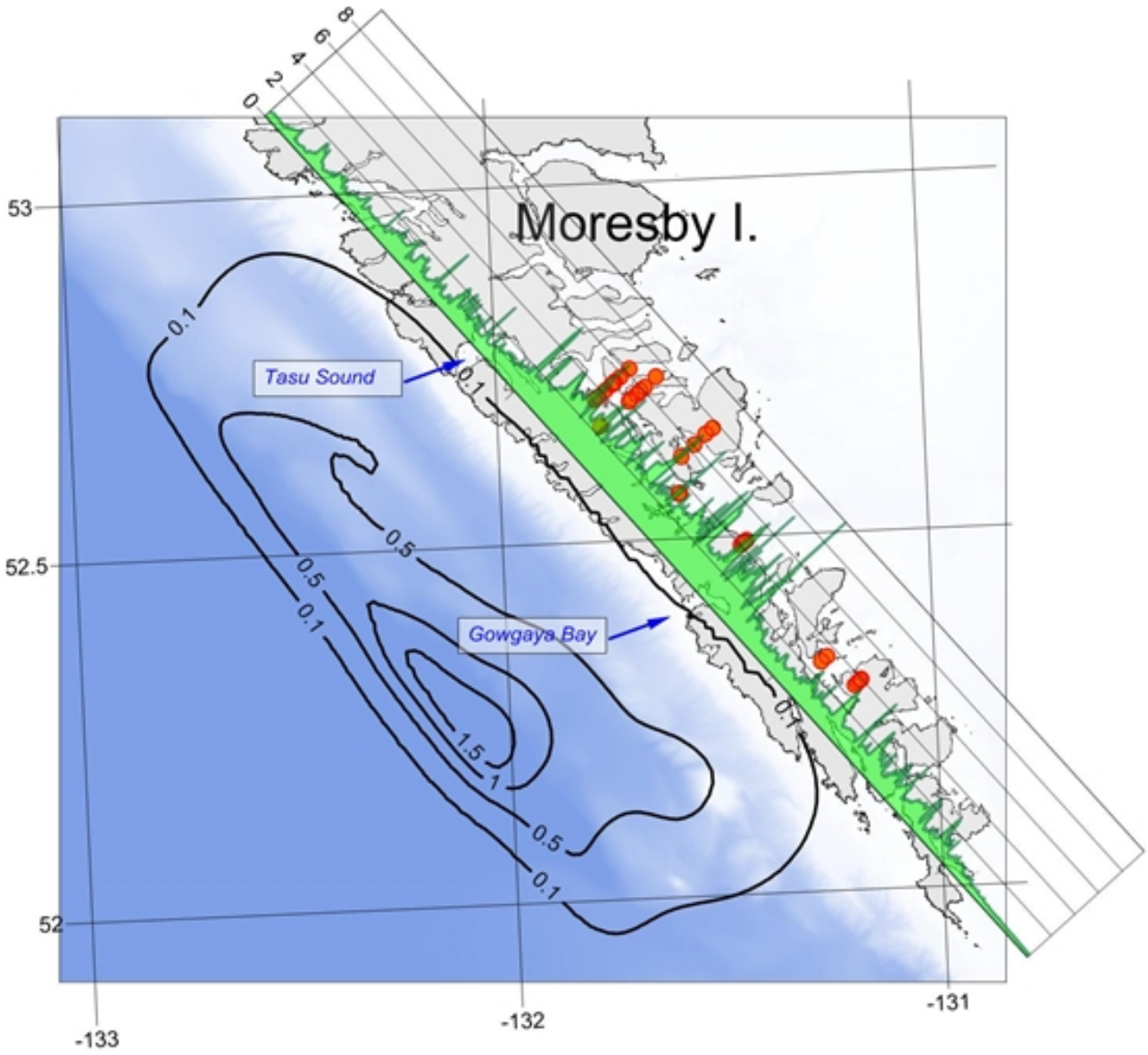

Figure 6.26: *Comparison between the modelled maximum elevations (Fine et al., 2015; green line) and the maximum run-up heights in sheltered bays (Leonard and Bednarski, 2014; red circles) on the west coast of Moresby Island. Black contours show the initial tsunami source used in the model.*

6.2.10 Conclusions

The M_W 7.8 earthquake which struck offshore Haida Gwaii in October of 2012 was the largest thrust event to hit the region in recent Canadian history and cemented the belief that the islands are prone to a complex combination of transform and oblique subduction dynamics. The M_W 7.8 earthquake occurred on a shallow, north-east dipping fault below the QCF, and studies (of aftershock distribution, moment tensor and coulomb stress) suggest the stress along the QCF's seismic gap increased. Part of Moresby Island was measured to have moved over a metre to the south-west and the ground motion lasted roughly 90 s, triggering numerous landslides and the cessation of thermal spring activity, but resulted in only minor damage in the islands' communities. The earthquake also created the largest tsunami of 2012, globally, with run-ups of over 6 m above tidal levels in inlets along the western coast of Moresby Island and possibly as high as 13 m just north of Tasu Sound. Aftershocks lasted months and were distributed in two trends; one up-dip from the mainshock (exhibiting predominantly normal and some strike-slip mechanisms) and another along the trace of the QCF (with strike-slip motion). With help from the USGS, a ShakeMap was created from submissions to the "Did You Feel It?" section of the GSC and USGS web sites. Through scientific observation and interaction with the people of Haida Gwaii, NRCan scientists learned, and continue to learn, a great deal about the complicated tectonics and the resulting earthquakes of the remote, beautiful islands of Haida Gwaii, Canada.

6.2.11 Acknowledgements

It should be noted that several figures were generated with the aid of Generic Mapping Tools software (Wessel and Smith, 1998). The authors are grateful for the assistance they received from colleagues (at NRCan), and associates (at the USGS), including the terrestrial and marine field crews. We are appreciative of Andreas Rosenberger for the data and discussion surrounding the strong-motion recordings. And, we acknowledge the valuable contribution of reviewers Malaika Ulmi, Nicky Hastings and Wayne Richardson. Finally, we respectfully thank the people of Haida Gwaii who took the time to share their experiences, and who helped the first author and NRCan field crews during their time on the islands, particularly Parks Canada and the First Nation Peoples of Haida Gwaii who assisted in GPS and seismic field deployments. This is Earth Sciences Sector (ESS) contribution number 20150358.

6.2.12 References

Akkar, S., M.A. Sandıkkaya, and J.J. Bommer (2014). Empirical ground-motion models for point- and extended-source crustal earthquake scenarios in Europe and the Middle East, *Bulletin of Earthquake Engineering*, **12**: 359–387, doi: 10.1007/s10518-013-9461-4.

Allen, T. I., and C. Brillon (2015). Assessment of Ground-Motion Models for use in the British Columbia North Coast Region, Canada, *Bulletin of the Seismological Society of America*, **105**: 1193-1205, doi: 10.1785/0120140266.

Allen, T. I., D. J. Wald, A. J. Hotovec, K. Lin, P. S. Earle, and K. D. Marano (2008). An Atlas of ShakeMaps for selected global earthquakes, *United States Geological Survey Open-File Report* 2008-1236 Open-File Report 2008-1236, Golden, 47 pp.

Atkinson, G. M. (2005). Ground motions for earthquakes in southwestern British Columbia and northwestern Washington: Crustal, in-slab, and offshore events, *Bulletin of the Seismological Society of America*, **95**: 1027–1044, doi: 10.1785/0120040182.

Atkinson, G. M., and J. Adams (2013). Ground motion prediction equations for application to the 2015 Canadian national seismic hazard maps, *Canadian Journal of Civil Engineering*, **40**: 988–998, dx.doi.org/10.1139/cjce-2012-0544.

Barrie, J.V., K.W. Conway, and P.T. Harris (2013). The Queen Charlotte Fault, British Columbia: seafloor anatomy of a transform fault and its influence on sediment processes. *Geo-Marine Letters*, **33**: 311-318, doi:10.1007/s00367-013-0333-3.

Bird, A. L., and M. Lamontagne (2015a). Impacts of the October 2012 Magnitude 7.8 Earthquake near Haida Gwaii, Canada, *Bulletin of the Seismological Society of America* (in press), doi: 10.1785/0120140167.

Bird, A. L., and M. Lamontagne (2015b). How Scientists' Communications helped mitigate the Psychosocial Effects of the October 2012 Magnitude 7.8 Earthquake near Haida Gwaii, Canada, *Seismological Research Letters*, **86**: 1301-1309,doi: 10.1785/0220140231.

Bird, A.L., G. C. Rogers, and G. D. Spence (1997). Earthquakes in the Queen Charlotte Islands Region: 1984-1996. *Lithoprobe Seismic Processing Facility Newsletter*, **10.1**: 39-44.

Bird, A.L. (1997). Earthquakes in the Queen Charlotte Islands Region: 1982 – 1996; Master of Science Thesis, University of Victoria, Victoria, BC, 134 pp. `http://www.collectionscanada.gc.ca/obj/s4/f2/dsk2/tape17/PQDD_0001/MQ34480.pdf`.

Bostwick, T. K. (1984). A Re-examination of the August 22, 1949 Queen Charlotte Earthquake: Master of Science Thesis, University of British Columbia, Vancouver, BC, 115 pp.

Cassidy, J. F., G. C. Rogers, and R. D. Hyndman (2014). An overview of the 28 October 2012 M_W 7.7 Earthquake in Haida Gwaii, Canada: A Tsunamigenic Thrust Event Along a Predominantly Strike-Slip Margin, *Pure and Applied Geophysics*, 1-9, doi: 10.1007/s00024-014-0775-1.

CBC (2014). "Haida Gwaii hot springs show more signs of returning", by Marissa Harvey, 06 June 2014: `http://www.cbc.ca/news/canada/british-columbia/haida-gwaii-hot-springs-show-more-signs-of-returning-1.2667320` (last accessed June 2014).

Chiou, B. S.-J., and R. R. Youngs (2008). An NGA model for the average horizontal component of peak ground motion and response spectra, *Earthquake Spectra* **24**: 173–215, doi: 10.1193/1.2894832.

Clague, J., J. R. Harper, R. J. Hebda, and D. E. Howes (1982). Late Quaternary sea levels and crustal movements, coastal British Columbia, *Canadian Journal of Earth Science*, **19**: 597-618, doi: 10.1139/e82-048.

Council of the Haida Nation (2015). "Hot pools filling at Gandll K'in Gwaay.yaay (Hotspring Island)!", by haidanation, 13 November 2015: `https://haidanation.wordpress.com/2015/11/13/hot-pools-filling-at-g%cc%b2andl-kin-gwaay-yaay-hotspring-island/` (last accessed December 2015).

DeMets, C., R. G. Gordon, D. F. Argus, and S. Stein (1990). Current Plate Motions, *Geophysical Journal International*, **101**: 425-478.

DeMets, C., R. G. Gordon, and D. F. Argus (2010). Geologically current plate motions, *Geophysical Journal International*, **181**: 1-80, doi: 10.1111/j.1365-246X.2009.04491.x.

Dengler, L. A., and J. W. Dewey (1998). An Intensity Survey of Households Affected by the Northridge, California, Earthquake of 17 January, 1994, *Bulletin of the Seismological Society of America*, **88**: 441-462.

Electric Power Research Institute (2003). CEUS Ground Motion Project: Model Development and Results, Palo Alto, CA, 105 pp.

Farahbod, A. M., and H. Kao (2015).Spatiotemporal Distribution of Events during the First Week of the 2012 Haida Gwaii Aftershock Sequence, *Bulletin of the Seismological Society of America*, **105**: 1231-1240, doi:10.1785/0120140173.

Fine, I. V., J. Y. Cherniawsky, R. E. Thomson, A. B. Rabinovich, and M. V. Krassovski (2015). Observations and numerical modeling of the 2012 Haida Gwaii tsunami off the coast of British Columbia, *Pure and Applied Geophysics*, doi: 10.1007/s00024-014-1012-7.

Gomberg, J. (2013). Permanently enhanced dynamic triggering probabilities as evidenced by two M 7.5 earthquakes. *Geophysical Research Letters*, **40**: 4828–4833, doi: 10.1002/grl.50933.

Hayes, G. (2013). Updated Finite Fault Results for the Oct 28, 2012 M_W 7.8 141 km S of Masset, Canada, Earthquake (Version 2): `http://comcat.cr.usgs.gov/earthquakes/eventpage/pde20121028030408820_14#scientific_finite-fault` (last accessed January 2015).

Hobbs, T. E., J. F. Cassidy, S. E. Dosso, and C. Brillon (2015a). Coulomb stress changes following the M_W 7.8 2012 Haida Gwaii, Canada earthquake: Implications for seismic hazard, *Bulletin of the Seismological Society of America*, **105**: 1253-1264, doi: 10.1785/0120140158.

Hobbs, T. E., J .F. Cassidy, and S. E. Dosso (2015b). Rupture properties of the M_W 7.8 2012 Haida Gwaii Earthquake from an Empirical Green's Function Method, *Bulletin of the Seismological Society of America*, **105**: 1219-1230, doi: 10.1785/0120140175.

Hu, Y., and K. Wang (2012). Spherical-Earth finite element model of short-term postseismic deformation following the 2004 Sumatra earthquake, *Journal of Geophysical Research*, **117**: B05404, doi: 10.1029/2012JB009153.

Hurwitz, S., R. A. Sohn, K. Luttrell, and M. Manga (2014). Triggering and modulation of geyser eruptions in Yellowstone National Park by earthquakes, earth tides, and weather, *Journal of Geophysical Research: Solid Earth*, **119**: 1718-1737, doi: 10.1002/2013JB010803.

Husen, S., R. Taylor, R. B. Smith, and H. Healser (2004). Changes in geyser eruption behavior and remotely triggered seismicity in Yellowstone National Park produced by the 2002 M7.9 Denali fault earthquake, Alaska: *Geology*, **32**: 537–540, doi: 10.1130/G20381.1.

Hutchinson, R. A. (1985). Hydrothermal changes in the Upper Geyser Basin, Yellowstone National Park, after the 1983 Borah Peak, Idaho, earthquake, in Proceedings of Workshop 28 on the 1983 Borah Peak, Idaho, Earthquake: *U.S. Geological Survey Open-File Report*, **85-290-A**: 612–624.

Hyndman, R. D. (2015). Tectonics and Structure of the Queen Charlotte Fault Zone, Haida Gwaii, and Large Thrust Earthquakes, *Bulletin of the Seismological Society of America*, **105**: 1058-1075, doi: 10.1785/0120140181

James, T., G. C. Rogers, J. F. Cassidy, H. Dragert, R. Hyndman, L. Leonard, L. Nykolaishen, M. Riedel, M. Schmidt, and K. Wang (2013). Field studies target 2012 Haida Gwaii earthquake, *EOS Transactions of the American Geophysical Union*, **94 (22)**: 197-198, doi: 10.1002/2013EO220002.

Kao, H., S.-J. Shan, A. Bent, C. Woodgold, G. Rogers, J. F. Cassidy, and J. Ristau (2012). Regional centroid-moment-tensor analysis for earthquakes in Canada and adjacent regions: an update, *Seismological Research Letters*, **83**: 505-515, doi: 10.1785/gssrl.83.3.505.

Kao, H., S.-J. Shan, and A. M. Farahbod (2015). Source characteristics of the 2012 Haida Gwaii earthquake sequence, submitted to the 2012 Haida Gwaii Special Volume, *Bulletin of the Seismological Society of America*, **105**: 1206-1218, doi: 10.1785/0120140165

Lamontagne, M., S. Halchuk, J. F. Cassidy, and G. C. Rogers (2008). Significant Canadian Earthquakes of the period 1600-2006. *Seismological Research Letters*, **79**: 211-223, doi: 1.1785/gssrl.79.2.211.

Lay, T., L., Ye, H. Kanamori, Y. Yamazaki, K. F. Cheung, K. Kwong, and K. D. Koper (2013). The October 28, 2012 M_W 7.8 Haida Gwaii underthrusting earthquake and tsunami: Slip partitioning along the Queen Charlotte Fault transpressional plate boundary. *Earth and Planetary Science Letters*, **375**: 57–70, doi: 10.1016/j.epsl.2013.05.005.

Leonard, L. J., and Bednarski, J. M. (2014). Field survey following the 28 October 2012 Haida Gwaii tsunami, *Pure and Applied Geophysics*, **171**: 3467-3482, doi: 10.1007/s00024-014-0792-0.

Leonard, L. J., and J. M. Bednarski (2015). The Preservation Potential of Coastal Coseismic and Tsunami Evidence Observed Following the 2012 M_W 7.8 Haida Gwaii Thrust Earthquake, *Bulletin of the Seismological Society of America*, **105**: 1280-1289, doi:10.1785/0120140193.

Millard, T. (2012). Landslides associated with the October 27, 2012 earthquake in Haida Gwaii, *Memorandum of the BC Ministry of Forests, Lands and Natural Resource Operations*, 9 pp.

Millard, T., M. Geertsema, J. J. Clague, P. Bobrowsky, A. Hasler, and M. Sakals (2012). Landslides on Haida Gwaii during and after the Earthquake, *Risky Ground*, **winter edition**: 12-13.

Milne, W.G. (1956). Seismic activity in Canada west of the 113° meridian, 1841-1951: *Publications of the Dominion Observatory*, Ottawa, **18**: 119-145.

National Geophysical Data Center/World Data System (NGDC/WDS) Global Historical Tsunami Database, Boulder, CO, USA. Available at: `http://www.ngdc.noaa.gov/hazard/tsu_db.shtml` (last accessed October 2013).

Natural Resources Canada / Geological Survey of Canada's "Did you feel it?" reports: `http://www.earthquakescanada.ca` (last accessed 27 January 2015).

Nykolaishen, L., H. Dragert, K. Wang, T. James, and M. Schmidt (2015). GPS Observations of Crustal Deformation Associated with the 2012 M_W 7.8 Haida Gwaii Earthquake, *Bulletin of the Seismological Society of America*, **105**: 1241-1252, doi:10.1785/0120140177.

Ottemöller, L., P. Voss, and J. Havskov (2012). SEISAN Earthquake Analysis Software, University of Bergen.

Ozawa, S., T. Nishimura, H. Munekane, H. Suito, T. Kobayashi, M. Tobia, and T. Imakiire (2012). Preceding, coseismic, and postseismic slips of the 2011 Tohoku earthquake, Japan. *Journal of Geophysical Research*, **117**: B07404, doi: 10.1029/2011JB009120.

Rinehart, J.S. (1972). Fluctuations in geyser activity caused by variations in earth tidal forces, barometric pressure, and tectonic stress, *Journal of Geophysical Research*, **77**: 342–350.

Ristau, J., G. C. Rogers, and J. F. Cassidy (2007). Stress in western Canada from regional moment tensor analysis, *Canadian Journal of Earth Sciences*, **44**: 127-148, doi: 10.1139/e06-057.

Roberts, R. G., A. Christoffersson, and F. Cassidy (1989). Real-time event detection, phase identification and source location estimation using single station three-component seismic data, *Geophysics Journal International*, **97**: 471-480.

Rohr, K. (2015). Plate boundary adjustment of the southernmost Queen Charlotte fault. *Bulletin of the Seismological Society of America*, **105**: 1076-1089, doi: 10.1785/0120140162.

Rogers, G. C. (1986). Seismic gaps along the Queen Charlotte Fault. *Earthquake Prediction Research*, **4**: 1–11.

Rosenberger, A., A. Bird, M. E. Turek, S. Huffman, G. Rogers, J. Cassidy, and T. Mulder (2013). Strong motion data from the magnitude 7.7 "Haida Gwaii" earthquake on October 27, 2012 (local time). *Geological Survey of Canada Open File 7324*, 35 pp, doi: 10.4095/292275.

Sun, T., K. Wang, T. Iinuma, R. Hino, J. He, H. Fujimoto, M. Kido, Y. Osada, S. Miura, Y. Ohta, and Y. Hu (2014). Prevalence of viscoelastic relaxation after the 2011 Tohoku-oki earthquake. *Nature*, **514**: 84-87, doi:10.1038/nature13778.

United States Geological Survey's "Did you feel it?" reports: `http://earthquake.usgs.gov/research/dyfi` (last accessed 27 January 2015).

Wald, D. J., V. Quitoriano, B. Worden, M. Hopper, and J. W. Dewey (2011). USGS "Did You Feel It?" Internet-based macroseismic intensity maps; *Annals of Geophysics*, **54**: 688-707, doi: 10.4401/ag-5354 plus appendix.

Wald, D. J., and T. I. Allen (2007). Topographic slope as a proxy for seismic site conditions and amplification, *Bulletin of the Seismological Society of America*, **97**: 1379-1395, doi: 10.1785/0120060267.

Wald, D. J., P. S. Earle, K. Lin, V. Quitoriano, and B. Worden (2006). Challenges in rapid ground motion estimation for the prompt assessment of global urban earthquakes, *Bulletin of the Earthquake Research Institute*, **81**: 272-281.

Wald, D. J., V. Quitoriano, T. H. Heaton, H. Kanamori, C. W. Scrivner, and B. C. Worden (1999). TriNet "ShakeMaps": Rapid generation of peak ground-motion and intensity maps for earthquakes in southern California, *Earthquake Spectra*, **15**: 537-556, doi: 10.1193/1.1586057.

Wang, K., Y. Hu, and J. He (2012). Deformation cycles of subduction earthquakes in a viscoelastic Earth. *Nature*, **484**: 327-332, doi: 10.1038/nature11032.

Wessel, P., and W. H. F. Smith (1998). New, improved version of the Generic Mapping Tools Released, *EOS Transactions, AGU*, **79**: 579, doi: 10.1029/98EO00426.

Worden, C. B., M. C. Gerstenberger, D. A. Rhoades, and D. J. Wald (2012). Probabilistic relationships between ground-motion parameters and Modified Mercalli Intensity in California, *Bulletin of the Seismological Society of America*, **102**: 204-221, doi: 10.1785/0120110156.

Worden, C. B., D. J. Wald, T. I. Allen, K. Lin, D. Garcia, and G. Cua (2010). A revised ground-motion and intensity interpolation scheme for ShakeMap, *Bulletin of the Seismological Society of America*, **100**: 3083–3096, doi: 10.1785/0120100101.

Zhao, J. X., J. Zhang, A. Asano, Y. Ohno, T. Oouchi, T. Takahashi, H. Ogawa, K. Irikura, H. K. Thio, P. G. Somerville, Y. Fukushima, and Y. Fukushima (2006). Attenuation relations of strong ground motion in Japan using site classification based on predominant period, *Bulletin of the Seismological Society of America*, **96**: 898–913, doi: 10.1785/0120050122.